

AD-A059 517

SCIENCE APPLICATIONS INC MCLEAN VA
A SIGMA COORDINATE OCEAN FORECASTING COMPUTER CODE. I. MODEL DI--ETC(U)
JAN 78 W J GRABOWSKI, G O ROBERTS
SAI-78-721-WA

F/G 8/3

N00014-77-C-0770

NL

UNCLASSIFIED

1 OF 2
AD
A059517

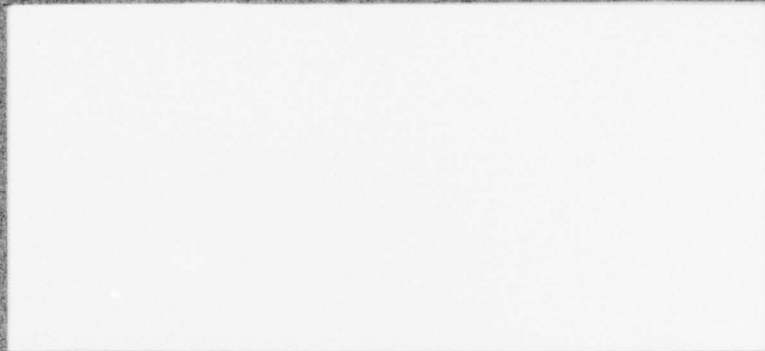


AD A0 595 17

DDC FILE COPY

LEVEL III

12



DDC
OCT 2 1978
RESERVED

This document has been approved
for public release and sale; its
distribution is unlimited.

SCIENCE APPLICATIONS, INC.

78 08 18 076

12

LEVEL #

DDC FILE COPY AD A0 59517

6

A SIGMA COORDINATE OCEAN
FORECASTING COMPUTER CODE

I. MODEL DIFFERENTIAL EQUATIONS, SPATIAL
FINITE-DIFFERENCE REPRESENTATION AND
CONSERVATION PROPERTIES.

9 Final rept. 15 Aug 77-15 Jan 78,

10 Walter J. Grabowski
Glyn O. Roberts

14 SAI-78-721-WA

11 15 Jan 78

12 121e

15 N00014-77-C-0770

DDC
OCT 2 1978

This document has been approved
for public release and sale; its
distribution is unlimited.



ATLANTA • ANN ARBOR • BOSTON • CHICAGO • CLEVELAND • DENVER • HUNTSVILLE • LA JOLLA
LITTLE ROCK • LOS ANGELES • SAN FRANCISCO • SANTA BARBARA • TUCSON • WASHINGTON

78 08 18 076

408 404

JOB

SAI-78-721-WA

A SIGMA COORDINATE OCEAN
FORECASTING COMPUTER CODE

I. MODEL DIFFERENTIAL EQUATIONS, SPATIAL
FINITE-DIFFERENCE REPRESENTATION AND
CONSERVATION PROPERTIES

Walter J. Grabowski
Glyn O. Roberts

15 January 1978

Final Report

Prepared for
Office of Naval Research
800 N. Quincy Street
Arlington, VA 22101

Naval Ocean Research and Development Activity
NSTL Station
Bay St. Louis, MS. 39529

SCIENCE APPLICATIONS, INC.

8400 Westpark Drive
McLean, Virginia 22101
(703) 821-4300

REPORT DOCUMENTATION PAGE		READ INSTRUCTIONS BEFORE COMPLETING FORM
1. REPORT NUMBER	2. GOVT ACCESSION NO.	3. RECIPIENT'S CATALOG NUMBER
4. TITLE (and Subtitle) A SIGMA COORDINATE OCEAN FORECASTING COMPUTER CODE I. MODEL DIFFERENTIAL EQUATIONS, SPATIAL FINITE-DIFFERENCE REPRESENTATION AND CONSERVATION PROPERTIES		5. TYPE OF REPORT & PERIOD COVERED Final, 8/15/77 - 1/15/78
7. AUTHOR(s) Walter J. Grabowski Glyn O. Roberts		6. PERFORMING ORG. REPORT NUMBER SAI-78-721-WA
9. PERFORMING ORGANIZATION NAME AND ADDRESS SCIENCE APPLICATIONS, INC. 8400 Westpark Drive McLean, VA. 22101		8. CONTRACT OR GRANT NUMBER(s) N00014-77-C-0770
11. CONTROLLING OFFICE NAME AND ADDRESS Office of Naval Research 800 N. Quincy Street, Arlington, VA 22101		10. PROGRAM ELEMENT, PROJECT, TASK AREA & WORK UNIT NUMBERS
14. MONITORING AGENCY NAME & ADDRESS (if different from Controlling Office) Naval Ocean Research & Development Activity NSTL Station, Bay St. Louis, MS. 39529 ATTN: Dr. S. A. Piacsek		12. REPORT DATE 15 January 1978
		13. NUMBER OF PAGES 123
		15. SECURITY CLASS. (of this report) Unclassified
		15a. DECLASSIFICATION/DOWNGRADING SCHEDULE N.A.
16. DISTRIBUTION STATEMENT (of this Report)		
<div style="border: 1px solid black; padding: 5px; width: fit-content; margin: 0 auto;"> <p>DISTRIBUTION STATEMENT A</p> <p>Approved for public release; Distribution Unlimited</p> </div>		
17. DISTRIBUTION STATEMENT (of the abstract entered in Block 20, if different from Report)		
18. SUPPLEMENTARY NOTES		
19. KEY WORDS (Continue on reverse side if necessary and identify by block number)		
Numerical Ocean Forecasting Ocean Circulation Modeling Sub-Grid Transport Parameterization Numerical Fluid Dynamics		Stratified Flow
20. ABSTRACT (Continue on reverse side if necessary and identify by block number)		
<p>In this report we describe results of the first phase of the development of an ocean forecasting finite-difference computer code. We first present a careful derivation of the model differential equations of mass, heat, salt and momentum conservation. They include parameterizations of the effects of heat, salt and momentum transport by motions which will not be resolved in the finite-difference representation. The model equations are</p>		

(cont'd)

DD FORM 1473
1 JAN 73EDITION OF 1 NOV 65 IS OBSOLETE
S/N 0102-LF-014-6501

SECURITY CLASSIFICATION OF THIS PAGE (When Data Entered)

* is presented first.

→ written in terms of a "sigma" coordinate system to simplify the treatment of bottom topography, coasts and islands. We also propose a set of surface, bottom and lateral boundary conditions, and we discuss the integral properties of the model equations, *are discussed.*

are proposed We then describe the spatial finite-difference representation of the model equations. It is based on a "box" approach and the problem variables are arranged on a staggered mesh system. We include the option for a non-uniform horizontal mesh system. The finite-difference equations are second-order accurate and they satisfy several important integral properties. The characteristics of "vector processing" computers, such as the Texas Instruments Advanced Scientific Computer, have been taken into consideration in the difference scheme development.

The implicit treatment of the temporal variation of the model equations and a detailed discussion of the sub-grid transport parameterization are included in two accompanying reports.

ACKNOWLEDGMENT

The authors would like to thank Ms. Barbara B. Czika for her patient and careful preparation of this manuscript and for her editorial assistance.

ACCESSION for	_____	_____
NTIS	_____	<input checked="" type="checkbox"/>
DDC	_____	<input type="checkbox"/>
UNCLASSIFIED	_____	<input type="checkbox"/>
J. S. 100 177	_____	_____
DISCONTINUITY CODES	_____	_____
A	_____	SPECIAL

TABLE OF CONTENTS

		<u>Page</u>
Section 1	INTRODUCTION	1-1
	1.1 MOTIVATION FOR AN OCEAN FORECASTING COMPUTER MODEL	1-1
	1.2 OCEAN FORECASTING MODEL REQUIREMENTS	1-3
	1.3 THE SAI/NORDA SIGMA COORDINATE MODEL	1-4
Section 2	OCEAN FORECASTING MODEL EQUATIONS	2-1
	2.1 OCEAN FORECASTING DIFFERENTIAL EQUATIONS	2-1
	2.1.1 MODEL VARIABLES AND PARAMETERS AND THE BOUSSINESQ APPROXIMATION	2-2
	2.1.2 AN ORTHOGONAL CURVI- LINEAR COORDINATE SYSTEM	2-3
	2.1.3 PARAMETERIZATION OF TRANSPORT DUE TO SMALL- SCALE MOTION	2-5
	2.1.4 THIN-LAYER AND HYDRO- STATIC APPROXIMATIONS	2-10
	2.1.5 GEOMETRIC SIMPLIFICATION	2-10
	2.1.6 SIGMA COORDINATES	2-14
	2.2 EQUATION OF STATE	2-23
	2.3 MODIFICATIONS TO ALLEVIATE ROUNDING ERROR	2-26
	2.3.1 INTRODUCTION OF REFERENCE STATE DENSITY AND PRESSURE	2-26
	2.4 USER-SPECIFIED POLES	2-29
	2.5 BOUNDARY CONDITIONS	2-31

TABLE OF CONTENTS
(Continued)

		<u>Page</u>
	2.5.1 OCEAN SURFACE CONDITIONS	2-31
	2.5.2 OCEAN BOTTOM CONDITIONS	2-33
	2.5.3 NO-FLUX LATERAL BOUNDARY CONDITIONS	2-36
	2.5.4 FLUX LATERAL BOUNDARY CONDITIONS	2-37
	2.5.5 PERIODICITY CONDITIONS IN LONGITUDE	2-39
	2.6 INTEGRAL PROPERTIES OF THE MODEL EQUATIONS	2-41
	2.7 OCEAN FORECASTING MODEL SUMMARY	2-44
Section 3	SPATIAL FINITE-DIFFERENCE REPRESENTATION	3-1
	3.1 THE FINITE-DIFFERENCE GRID SYSTEM	3-3
	3.1.1 THE GRID SYSTEM	3-3
	3.1.2 ARRANGEMENT OF DEPENDENT VARIABLES	3-8
	3.2 THE FINITE-DIFFERENCE EQUATIONS	3-12
	3.2.1 THE CONTINUITY EQUATION	3-14
	3.2.2 HEAT AND SALT EQUATIONS	3-15
	3.2.3 HORIZONTAL MOMENTUM EQUATIONS AND THE HYDRO- STATIC RELATION	3-19
	3.2.4 THE EQUATION OF STATE	3-25
	3.3 THE BOUNDARY CONDITIONS	3-26
	3.3.1 EXTERIOR MESH LINES	3-26
	3.3.2 OCEAN SURFACE BOUNDARY CONDITIONS	3-28

TABLE OF CONTENTS
(Continued)

	<u>Page</u>
3.3.3 OCEAN BOTTOM BOUNDARY CONDITIONS	3-31
3.3.4 NO-FLUX LATERAL BOUNDARY CONDITIONS	3-32
3.3.5 FLUX LATERAL BOUNDARY CONDITIONS	3-34
3.3.6 PERIODICITY CONDITIONS IN LONGITUDE	3-35
Section 4 DIFFERENCE-SCHEME CONSERVATION PROPERTIES	4-1
4.1 SUMMATION DEFINITIONS AND RELATIONS	4-1
4.2 CONSERVATION OF VT AND VS (CONSERVATION PROPERTY 1)	4-6
4.3 CONSERVATION OF VT^2 AND VS^2 BY ADVECTION (CONSERVATION PROPERTY 2)	4-9
4.4 CONSERVATION OF HORIZONTAL KINETIC ENERGY BY ADVECTION, AND CONVERSION OF KINETIC ENERGY TO POTENTIAL ENERGY (CONSERVATION PROPERTIES 3 AND 4).	4-12
Section 5 SUMMARY AND CONCLUDING REMARKS	5-1
Section 6 REFERENCES	6-1

LIST OF FIGURES

	<u>Page</u>
Figure 1	BASIC FINITE-DIFFERENCE GRID SYSTEM IN LATERAL PLANE 3-4
Figure 2	ARRANGEMENT OF VARIABLES AND T-S GRID CELL 3-9
Figure 3	THE u-v GRID CELL 3-13
Figure 4	ARRANGEMENT OF FINITE-DIFFERENCE SUB- GRID HEAT (AND SALT) FLUXES, RATE OF STRAIN COMPONENTS, AND HORIZONTAL AND VERTICAL DIFFUSIVITIES IN CONSTANT σ PLANE 3-17

LIST OF TABLES

Table 2.1	SUMMARY OF OCEAN FORECASTING MODEL EQUATIONS 2-45
Table 4.1	SUMMATION RELATIONS 4-3

Section 1
INTRODUCTION

1.1 MOTIVATION FOR AN OCEAN FORECASTING COMPUTER MODEL

As the sensitivity and effective range of acoustic detection and weapon systems increases, knowledge of the detailed oceanic environment in which these systems operate becomes increasingly important. At present, however, the Navy has no capability to forecast ocean environmental conditions, and detection and weapon system performance predictions depend upon coarse analyses of historic and synoptic data. The Navy Oceanographic Prediction System (OPS) has been proposed in response to the growing need for such a capability. The purpose of OPS is to provide accurate five-day predictions of the major characteristics of whole-ocean regions, and two-day predictions in greater detail in smaller regions. In many ways OPS will be similar to the atmospheric prediction computer models which have been developed over the last 10 to 15 years.

When its development is completed, OPS will be integrated into the Primary Environmental Processing System (PEPS) at the U.S. Naval Fleet Numerical Weather Central. It will there interface with a data analysis and initialization system, an atmospheric prediction computer model, and ocean-surface wave forecasting models to provide a dynamic description of the total marine environment.

In this report and two accompanying reports (Roberts and Grabowski, 1978a; Roberts and Grabowski, 1978b), we describe the SAI/NORDA ocean forecasting model. We believe this model has the features and flexibility to form the basis of the Oceanographic Prediction System.

1.2 OCEAN FORECASTING MODEL REQUIREMENTS

The capabilities required of the ocean forecasting model when fully developed are described in the document "Operational Requirement: Oceanographic Prediction System" drafted by the Director of Naval Oceanography and Meteorology in 1977. The requirements include:

- Variable horizontal mesh resolution from 100 km for global predictions to 1 km over areas of 3×10^4 km².
- The ability to operate both in a basic coarse-mesh mode over large areas, and in a nested fine-mesh mode which can result in detailed predictions within small areas of high interest.
- Minimum prediction performance criteria of temperature to 0.5°C, horizontal temperature gradients to 0.25°C/km, current speed to 5% and direction to 10°, and salinity to 0.05 gm/kg.

We have used these requirements as guides throughout the first stage of model development, which we describe in this and the two accompanying reports, and we will continue to do so as our development effort proceeds. We expect satisfaction of these requirements will require a finite-difference model with between 15 and 20 vertical mesh levels.

The SAI/NORDA Sigma Coordinate Ocean Forecasting Model is based on the "primitive equations" and it includes the following features:

- Dynamic predictive equations for the temperature, salinity, density, and the three components of current velocity as functions of location and depth.
- A sigma vertical-coordinate system to simplify the treatment of bottom topography, coasts and islands.
- A parameterization of transport due to small-scale unresolvable motions based on gradient transport hypotheses and a variable, anisotropic eddy diffusivity.
- An option for user specification of the coordinate system poles.
- The ability to operate in global, hemispherical, whole-ocean, and limited region modes.
- Non-uniform mesh spacing to make most economic use of finite-difference mesh points.
- A stable, temporally implicit, second-order finite-difference representation of the model differential equations which allows large time steps and which satisfies important integral properties.
- A formulation of the difference-scheme, including boundary conditions, which is suitable for coding for "vector processing" computers such as the Texas Instruments Advanced Scientific Computer.

In this report we describe the derivation of the model differential equations, their spatial finite-difference representation including integral properties, and appropriate boundary conditions and their numerical implementation. The implicit finite-difference treatment of the temporal variation is described in Roberts and Grabowski (1978a). The parameterization of the transport effects of small-scale, unresolvable motion is discussed in Roberts and Grabowski (1978b).

Section 2

OCEAN FORECASTING MODEL EQUATIONS

2.1 OCEAN FORECASTING DIFFERENTIAL EQUATIONS

In this section we present the basic differential equations of the ocean forecasting model. We begin with the fundamental differential equations representing conservation of mass, heat, salt and momentum. The equations are expressed in a reference system rotating with the earth. The following six sections describe the derivation of the model differential equations in the following order:

1. We introduce basic model variables and parameters and apply the Boussinesq approximation.
2. We introduce a system of orthogonal curvilinear coordinates based on the earth's geopotential surfaces.
3. We present a parameterization of the heat, salt and momentum transport due to motions which will not be resolved in the finite-difference computations.
4. We apply a thin-layer assumption and make the hydrostatic approximation.
5. We perform a geometric simplification and neglect variations of the coordinate system metric coefficients from their spherical thin-layer counterparts.
6. We introduce a σ -coordinate system to simplify the treatment of bottom topography.

2.1.1 Model Variables and Parameters and the Boussinesq Approximation.

To the basic system of differential equations which represent conservation of mass, heat, salt and momentum, we apply the Boussinesq approximation so that we neglect density differences except in the buoyancy force term. The Boussinesq approximation is appropriate to the study of almost all oceanic motions (except the propagation of sound waves). The equations become

$$\nabla \cdot \underline{u} = 0 \quad , \quad (2.1a)$$

$$\dot{T} = - \nabla \cdot (\underline{u}T + \underline{q}) + \varepsilon + \phi \quad , \quad (2.1b)$$

$$\dot{S} = - \nabla \cdot (\underline{u}S + \underline{\gamma}) \quad , \quad (2.1c)$$

$$\begin{aligned} \dot{\underline{u}} = & - \nabla \cdot (\underline{u}; \underline{u} - \underline{\tau}) - 2\Omega \times \underline{u} - \nabla p / \rho_0 \quad , \\ & - \rho \nabla \chi / \rho_0 \quad , \quad (2.1d) \end{aligned}$$

and

$$\rho = \rho(T, S, p) \quad . \quad (2.2)$$

In these equations \underline{u} is the fluid velocity relative to the rotating reference frame, T is the temperature, S is the salinity (the mass fraction of salt), ρ is the density (water and salt) and p is the pressure. The heat source terms ε and ϕ represent the absorption of solar radiation and the generation of heat by viscous dissipation, respectively. The vector $\underline{\Omega}$ is the earth's angular velocity ($|\underline{\Omega}| = 7.292116 \times 10^{-5}$ radians/sec), χ is the effective gravitational potential (including the centrifugal potential),

and ρ_0 is a mean surface density. The equation of state (2.2) is included to complete the system.

The fluxes \underline{q} , $\underline{\gamma}$ and $\underline{\tau}$ arise from molecular diffusion; they are given by

$$\underline{q} = -\alpha \nabla T \quad ,$$

$$\underline{\gamma} = -D \nabla S \quad ,$$

and

$$\underline{\tau} = \nu \underline{e} \quad , \quad (2.3a-c)$$

where α , D and ν are appropriate molecular diffusivities, and the rate-of-strain tensor

$$\underline{e} = \frac{1}{2} [\nabla \underline{u} + (\nabla \underline{u})^T] \quad . \quad (2.3d)$$

We present a particularly useful coordinate system for the component expression of equations (2.1) and (2.3) in the following section.

2.1.2 An Orthogonal Curvilinear Coordinate System

We define a left-handed, orthogonal, curvilinear coordinate system (λ, ϕ, z) based on the earth's geopotential surfaces as follows. We let

$$z = (\chi_s - \chi)/g \quad , \quad (2.4)$$

where χ_s is the surface geopotential and g is an appropriate value of the apparent acceleration due to gravity, which

will be held fixed over the model extent. Thus z is approximately equal to the depth measured positive downward from the surface geopotential.* We next introduce surfaces of constant λ and ϕ such that the λ , ϕ and z surfaces are everywhere mutually orthogonal. We define the λ and ϕ surfaces uniquely by requiring that they coincide on the earth's surface geopotential with lines of constant longitude and latitude defined in the conventional manner in terms of the normal to the surface geopotential.

We now let u , v and w represent the components of \underline{v} in the λ , ϕ and z directions, respectively. We also let h_λ , h_ϕ , and h_z represent the corresponding metric coefficients where $h_\lambda d\lambda$ and $h_\phi d\phi$ are elements of distance along a geopotential surface in the east and north directions, and $h_z dz$ is the element of distance normal to the geopotentials. With these definitions we can express equations (2.1) and (2.3) in component form in the (λ, ϕ, z) coordinate system in terms of h_λ , h_ϕ and h_z and the general orthogonal curvilinear coordinate expressions for the gradient and divergence operators.

Since we have not yet derived expressions for the metric coefficients, it serves no useful purpose to present the component-form equations at this point. It is important to recognize, however, that as a result of our definition of z the gravitational force appears only in the z component of the momentum equation. In a following section we will propose approximate metric coefficients and present the component equations.

* The difference between actual depth and z will always be less than 0.3%.

2.1.3 Parameterization of Transport due to Small-Scale Motion.

A fundamental aspect of the approximation of differential equations by finite-difference equations is that components of the solution of the differential system with scales on the order of the difference-grid spacing, or smaller, cannot be resolved. If such small scale components make important contributions to the complete solution, then we can expect significant errors in our numerical solution. In many situations errors arising from inadequate resolution pose no real difficulty - we simply increase the resolution of our numerical solution by decreasing the finite-difference mesh widths. In typical oceanic flows, however, the scales of motion vary over such a wide range that, even with the largest existing or planned computers, resolution sufficient to resolve all of the significant scales is not possible. The ratio between the characteristic dimensions of the largest and smallest horizontal eddies in an ocean-sized region is approximately $1:5 \times 10^8$, and the ratio of the corresponding time scales is on the order of 1 sec: 1 yr. or $1:3 \times 10^7$ (Woods, 1977). A numerical model with sufficiently fine spatial resolution to resolve all of the scales of motion would therefore require on the order of $10^8 \times 10^8 \times 10^5$ spatial grid points (we have assumed that the smallest vertical motions also have a length scale of 1cm). The time step at which such a hypothetical numerical model could advance would be on the order of one second. Such a model is not feasible.

In this modeling effort we are interested, in general, in the large scale features of the ocean circulation, and we expect to be able to adequately resolve motions on such scales. Such features include the major current

systems and mesoscale eddies. Small-scale motions, however, may not be neglected since they are responsible for much of the horizontal transport of heat, salt and momentum and practically all of the vertical transport. Also, the dissipation of kinetic energy by viscous stresses operates at the smallest scales. In our model, therefore, we parameterize the effects of the small scale motions in terms of the large scale, resolved motion.

The parameterization of sub-grid scale motion is discussed in detail in an accompanying report (Roberts and Grabowski, 1978b) and only the basic results are presented here. In essence, each dependent variable is decomposed by a filtering process into a filtered part which consists of those components of the spatial variation of the variable with length scales greater than the mesh spacing, and a residual part which consists of the remaining small-scale components. The filtering process is also applied to the equations of motion. The procedure described here is similar to that followed in the more common Reynolds decomposition of the equations of motion except that temporal or ensemble averaging is replaced by filtering. A good discussion of filtering procedures is presented by Kwak, et al. (1975).

The filtered equations, expressed in terms of the filtered "grid-resolved" parts and residual or "sub-grid" scale parts of the dependent variables are identical to equations (2.1) (and to their representation in λ, ϕ, z coordinates) except that T, S, u, v, w, ρ and p represent their resolved-scale components, and the fluxes \underline{q} , $\underline{\gamma}$ and $\underline{\tau}$ now include additional terms (akin to Reynolds stresses) which represent heat, salt and momentum transport due to the sub-grid scale motion.

We model the sub-grid scale fluxes following an eddy diffusivity hypothesis. From this point, we will ignore the effects of molecular viscosity so that

$$\phi = 0$$

and \underline{q} , $\underline{\gamma}$ and $\underline{\tau}$ consist only of the sub-grid flux contributions. The fluxes are modeled as follows:

$$\begin{aligned} (\underline{q})_H &= -\beta_H K_H (\nabla T)_H & , \\ (\underline{q})_V &= -\beta_V K_V (\nabla T)_V & , \end{aligned} \quad (2.5a, b)$$

$$(\underline{\tau})_{HH} = K_H (\underline{e})_{HH} & ,$$

$$(\underline{\tau})_{VH} = K_V (\underline{e})_{VH} & ,$$

and

$$(\underline{\tau})_{VV} = K_V (\underline{e})_{VV} & . \quad (2.6a-c)$$

The $\underline{\gamma}$ flux components are modeled in identical fashion to the \underline{q} fluxes. Subscript "H" refers to the horizontal, λ and ϕ , components of the vector or tensor, and "V" refers to the vertical component. The "VH" components of $\underline{\tau}$ are $\tau_{z\lambda}$ and $\tau_{z\phi}$.

The quantities K_H and K_V are eddy diffusivities for horizontal and vertical mixing and β_H and β_V are corresponding inverse Prandtl numbers. In oceanic flows, the motions which make the major contributions to horizontal mixing have much larger length scales (and time scales) than the motions responsible for vertical mixing. It is conceivable, in fact, that in some oceanic simulations the horizontal grid

resolution may be sufficient to resolve most of the important horizontal mixing motions; however, the grid resolution will never be fine enough to adequately resolve the important vertical mixing motions. Therefore, while our horizontal eddy diffusivity is a function of grid spacing and decreases as the grid spacing decreases (as more of the horizontal motion is resolved), our vertical diffusivity is independent of the grid spacing.

The horizontal eddy diffusivity K_H is similar to that proposed by Smagorinsky, et al. (1965),

$$K_H = (C_g \Delta)^2 (2e_{ij}e_{ji})^{\frac{1}{2}} \quad (2.7)$$

where i and j represent λ and ϕ , and the summation convention is assumed. The quantity C_g is an adjustable constant (about 0.1), and Δ is a characteristic horizontal finite-difference grid spacing.

The vertical diffusivity K_V is given by an approximation (Martin, 1976) to the Mellor-Yamada Level 2 diffusion model (Mellor and Yamada, 1972). We specify

$$K_V = \ell^2(z) \left[\left(\frac{\partial u}{\partial z} \right)^2 + \left(\frac{\partial v}{\partial z} \right)^2 \right]^{\frac{1}{2}} (1-R/R_c)^{3/2} \quad (2.8a)$$

where the Richardson number

$$R = N^2 / \left[\left(\frac{\partial u}{\partial z} \right)^2 + \left(\frac{\partial v}{\partial z} \right)^2 \right] \quad (2.8b)$$

and the critical Richardson number

$$R_c = 0.23 \quad (2.8c)$$

The quantity $l(z)$ is a suitable vertical turbulent length scale, and N is the Brunt-Vaisala frequency given by

$$N^2 = \frac{g}{\rho_0} \left[\left(\frac{\partial \rho}{\partial z} \right)_{\lambda, \phi} - \left(\frac{\partial \rho}{\partial p} \right)_{TS} \frac{\partial p}{\partial z} \right] \quad (2.8d)$$

where $(\partial \rho / \partial p)_{TS}$ is determined from the equation of state.* The Richardson number in (2.8) is a measure of the degree of balance between the stabilizing effect of the density gradient and the destabilizing effect of the flow shear. As R approaches its critical value R_c , the stabilizing effect overwhelms the destabilizing effect, no mixing can occur, and K_V goes to zero. We add a small exponentially decreasing vertical diffusivity $C_V \exp(-z/z_V)$ to account for those regions where K_V as given by (2.8) is very small or zero.

Appropriate values of β_H may be in the range 1.4 to 1.6 - typical values for unstratified turbulent shear flows (Launder, 1975). The experimental data of Webster (1964) taken in a stratified free-shear flow suggest that as R varies from 0. to 0.25, β_V varies from 1.6 to 1.0. The decrease in β_V as R increases is due to the fact that as R increases, the relative contribution of internal wave motions to the small-scale motion increases. Internal waves transport momentum but not heat and salt. Some dependence of β_V on R , based on the experimental data, will be included in the model.

With the specification of suitable boundary conditions, and an equation of state, we have a completely formulated problem suitable for numerical simulation. However, several important simplifications may be applied.

* To obtain (2.8d) we made use of the fact that to a good approximation the specific heat ratio of sea water is unity.

2.1.4 Thin-Layer and Hydrostatic Approximations.

We now proceed to simplify the complex, parameterized equations described in the previous sections. We assume that, in terms of the curvilinear coordinate system introduced above, scales of motion in the z-direction are much smaller than the corresponding scales in the λ and ϕ directions so that $w \ll u$ and v . This is a thin-layer approximation motivated by the fact that the lateral dimensions of ocean forecast regions will be much greater than region depths. We do not assume that derivatives in z of terms involving w are small. We also assume that in the z component of the momentum equation all of the terms involving velocity are small compared with the buoyancy and pressure gradient terms.

With the above assumptions, we reduce the z momentum equation to the hydrostatic relation

$$\frac{\partial p}{\partial z} = \rho g \quad , \quad (2.9)$$

and we neglect several terms involving w in the λ and ϕ components of the momentum equation.*

2.1.5 Geometric Simplification

To the complex system of equations derived as described in the four previous sections, we perform a final simplification. As of this point, the component equations are represented in terms of the undetermined metric

* To obtain (2.9) we make use of the fact that the vertical metric coefficient h_z is given by $g/|\nabla\chi|$.

coefficients h_λ , h_ϕ , and h_z . We make a thin-layer spherical-geometry approximation and neglect variations of h_λ and h_ϕ from their spherical thin-layer counterparts so that

$$h_\lambda = a \cos \phi \quad ,$$

and

$$h_\phi = a \quad , \quad (2.10a,b)$$

where a is the mean radius of the earth. The error introduced into the equation system by this approximation is negligible.

We further neglect the small difference between h_z and unity and replace $h_z = g/|\nabla\chi|$ by

$$h_z = 1 \quad . \quad (2.11)$$

The maximum difference between g and $|\nabla\chi|$ will always be less than 0.3%.

With these final simplifications and with the definition $f = 2\Omega \sin \phi$, the system of differential equations becomes:

$$\frac{\partial u}{\partial \lambda} + \frac{\partial}{\partial \phi}(v \cos \phi) + \frac{\partial}{\partial z}(w a \cos \phi) = 0 \quad , \quad (2.12a)$$

$$\begin{aligned} \dot{T} = & - \frac{1}{a \cos \phi} \left\{ \frac{\partial}{\partial \lambda} [uT + q_\lambda] + \frac{\partial}{\partial \phi} [(vT + q_\phi) \cos \phi] \right. \\ & \left. + \frac{\partial}{\partial z} [(wT + q_z) a \cos \phi] \right\} + \epsilon \quad , \quad (2.12b) \end{aligned}$$

$$\begin{aligned} \dot{S} = & - \frac{1}{a \cos \phi} \left\{ \frac{\partial}{\partial \lambda} [uS + \gamma_{\lambda}] + \frac{\partial}{\partial \phi} [(vS + \gamma_{\phi}) \cos \phi] \right. \\ & \left. + \frac{\partial}{\partial z} [(wS + \gamma_z) a \cos \phi] \right\} \end{aligned} \quad , \quad (2.12c)$$

$$\begin{aligned} \dot{u} = & - \frac{1}{a \cos \phi} \left\{ \frac{\partial}{\partial \lambda} [uu - \tau_{\lambda\lambda}] + \frac{\partial}{\partial \phi} [(vu - \tau_{\phi\lambda}) \cos \phi] \right. \\ & \left. + \frac{\partial}{\partial z} [(wu - \tau_{z\lambda}) a \cos \phi] \right\} \\ & + (vu - \tau_{\phi\lambda}) \frac{\tan \phi}{a} + vf - \frac{1}{\rho_0 a \cos \phi} \frac{\partial p}{\partial \lambda} \end{aligned} \quad , \quad (2.12d)$$

$$\begin{aligned} \dot{v} = & - \frac{1}{a \cos \phi} \left\{ \frac{\partial}{\partial \lambda} [uv - \tau_{\lambda\phi}] + \frac{\partial}{\partial \phi} [(vv - \tau_{\phi\phi}) \cos \phi] \right. \\ & \left. + \frac{\partial}{\partial z} [(wv - \tau_{z\phi}) a \cos \phi] \right\} \\ & - (uu - \tau_{\lambda\lambda}) \frac{\tan \phi}{a} - uf - \frac{1}{\rho_0 a} \frac{\partial p}{\partial \phi} \end{aligned} \quad , \quad (2.12e)$$

and

$$\frac{\partial p}{\partial z} = g\rho \quad . \quad (2.12f)$$

We obtain expressions for the sub-grid scale heat and salt fluxes in (2.12b) and (2.12c) from (2.5). To the spherical thin-layer approximation, the gradients of scalars such as T and S are given by

$$\nabla T = \frac{\hat{\lambda}}{a \cos \phi} \frac{\partial T}{\partial \lambda} + \frac{\hat{\phi}}{a} \frac{\partial T}{\partial \phi} + \hat{z} \frac{\partial T}{\partial z} ,$$

so that

$$q_{\lambda} = - \frac{\beta_H K_H}{a \cos \phi} \frac{\partial T}{\partial \lambda} ,$$

$$q_{\phi} = - \frac{\beta_H K_H}{a} \frac{\partial T}{\partial \phi} ,$$

and

$$q_z = - \beta_V K_V \frac{\partial T}{\partial z} , \quad (2.13a-c)$$

with similar expressions for γ_{λ} , γ_{ϕ} and γ_z .

The sub-grid scale momentum fluxes are obtained from (2.6). To the spherical thin-layer approximation, the five relevant components of the rate of strain tensor are

$$e_{\lambda\lambda} = \frac{2}{a \cos \phi} \left\{ \frac{\partial u}{\partial \lambda} - v \sin \phi \right\} ,$$

$$e_{\phi\lambda} = \frac{1}{a \cos \phi} \left\{ \frac{\partial v}{\partial \lambda} + \frac{\partial u}{\partial \phi} \cos \phi + u \sin \phi \right\} ,$$

$$e_{z\lambda} = \frac{\partial u}{\partial z} ,$$

$$e_{\phi\phi} = \frac{2}{a} \frac{\partial v}{\partial \phi} ,$$

and

$$e_{z\phi} = \frac{\partial v}{\partial z} , \quad (2.14a-e)$$

With these expressions the sub-grid scale stresses are given by

$$\tau_{\lambda\lambda} = K_H e_{\lambda\lambda} \quad ,$$

$$\tau_{\phi\lambda} = K_H e_{\phi\lambda} \quad ,$$

$$\tau_{z\lambda} = K_V e_{z\lambda} \quad ,$$

$$\tau_{\phi\phi} = K_H e_{\phi\phi} \quad ,$$

and

$$\tau_{z\phi} = K_V e_{z\phi} \quad . \quad (2.15a-e)$$

The horizontal diffusivity in the above expressions for the sub-grid fluxes is obtained from (2.7) and is expressed in terms of (2.14) as

$$K_H = (C_g \Delta)^2 \left[2(e_{\lambda\lambda}^2 + e_{\phi\phi}^2 + 2e_{\phi\lambda}^2) \right]^{\frac{1}{2}} \quad . \quad (2.16)$$

The vertical diffusivity is as given in (2.8)

We will express this system of model equations in terms of a new vertical variable σ as described in the next section.

2.1.6 Sigma Coordinates

In this section we introduce a new vertical coordinate σ to replace z such that as z varies from the surface to the bottom σ varies from zero to one.

The lateral region over which our ocean forecasting code is to be applied is always rectangular in λ and ϕ , and it is described by

$$\lambda_W \leq \lambda \leq \lambda_E \quad (2.17a)$$

and

$$\phi_S \leq \phi \leq \phi_N \quad (2.17b)$$

where the subscripts W, E, S and N represent the West, East, South and North boundaries, respectively. We specify that land areas which appear in the region, both along the boundaries and in the interior, be depressed and covered with a thin layer of water. In this way we avoid the problems associated with fitting a lateral mesh system to an irregular coast or about an island. These problems are especially severe when difference schemes are programmed for a "vector processing" computer such as the Texas Instruments ASC. The absorptivity of solar radiation of this overland water will be zero, as will the surface heat flux and the applied wind stress. The small fluxes of mass, heat, salt and momentum across land areas which may occur will not cause difficulties.

The vertical extent of the solution domain is

$$z_b \leq z \leq z_s \quad (2.17c)$$

where $z_b(\lambda, \phi)$ and $z_s(\lambda, \phi, t)$ are the ocean depth and surface elevation measured positive downward from the surface geopotential. An extensive data base exists for $z_b(\lambda, \phi)$ in all ocean regions. In order to simplify the numerical treatment of the differential equations, we apply a simple

transformation to z such that as z varies from z_s to z_b , a transformed variable σ varies from zero to one. We define

$$\sigma = \frac{\ln \left[1 + (z - z_s) / \delta \right]}{\ln \left[1 + (z_b - z_s) / \delta \right]} \quad (2.18)$$

The quantity δ is a parameter which can be adjusted to ensure that the finite-difference representation adequately resolves the vertical variation of the dependent variables in the upper ocean. As a result of our choice of transformation, a finite-difference grid system equi-spaced in σ expands geometrically with z , with spacing proportional to $\delta + z$.

To transform equations (2.8) and (2.12) through (2.15) to the sigma-coordinate system, we make use of the following results. Let f be any function of λ , ϕ and z , then in terms of λ , ϕ and σ , λ -derivatives of f are written, using the chain rule,

$$\left(\frac{\partial f}{\partial \lambda} \right)_z = \left(\frac{\partial f}{\partial \lambda} \right)_\sigma + \frac{\partial f}{\partial \sigma} \left(\frac{\partial \sigma}{\partial \lambda} \right)_z \quad (2.19a)$$

An elementary application of the chain rule yields

$$\left(\frac{\partial \sigma}{\partial \lambda} \right)_z \left(\frac{\partial \lambda}{\partial z} \right)_\sigma \left(\frac{\partial z}{\partial \sigma} \right)_\lambda = -1$$

so that

$$\left(\frac{\partial f}{\partial \lambda} \right)_z = \left(\frac{\partial f}{\partial \lambda} \right)_\sigma - \frac{\partial f}{\partial \sigma} \frac{\partial \sigma}{\partial z} \left(\frac{\partial z}{\partial \lambda} \right)_\sigma \quad (2.19b)$$

This last result may also be written as

$$\left(\frac{\partial f}{\partial \lambda}\right)_z = \frac{\partial \sigma}{\partial z} \left[\frac{\partial}{\partial \lambda} \left(f \frac{\partial z}{\partial \sigma} \right) - \frac{\partial}{\partial \sigma} \left(f \frac{\partial z}{\partial \lambda} \right) \right] \quad (2.19c)$$

with the λ -derivatives on the right-hand side taken with σ held fixed. Similarly

$$\begin{aligned} \left(\frac{\partial f}{\partial \phi}\right)_z &= \left(\frac{\partial f}{\partial \phi}\right)_\sigma + \frac{\partial f}{\partial \sigma} \left(\frac{\partial \sigma}{\partial \phi}\right)_z, \\ &= \left(\frac{\partial f}{\partial \phi}\right)_\sigma - \frac{\partial f}{\partial \sigma} \frac{\partial \sigma}{\partial z} \left(\frac{\partial z}{\partial \phi}\right)_\sigma, \\ &= \frac{\partial \sigma}{\partial z} \left[\frac{\partial}{\partial \phi} \left(f \frac{\partial z}{\partial \sigma} \right) - \frac{\partial}{\partial \sigma} \left(f \frac{\partial z}{\partial \phi} \right) \right]. \end{aligned} \quad (2.19d-f)$$

Derivatives in z transform simply as

$$\frac{\partial f}{\partial z} = \frac{\partial f}{\partial \sigma} \frac{\partial \sigma}{\partial z} \quad (2.20)$$

If f is also a function of t then

$$\left(\frac{\partial f}{\partial t}\right)_z = \left(\frac{\partial f}{\partial t}\right)_\sigma + \frac{\partial f}{\partial \sigma} \left(\frac{\partial \sigma}{\partial t}\right)_z \quad (2.21a)$$

From the chain rule, we can obtain

$$\left(\frac{\partial \sigma}{\partial t}\right)_z = -\left(\frac{\partial \sigma}{\partial z}\right)_t \left(\frac{\partial z}{\partial t}\right)_\sigma ,$$

so that

$$\left(\frac{\partial f}{\partial t}\right)_z = \left(\frac{\partial f}{\partial t}\right)_\sigma - \frac{\partial f}{\partial \sigma} \frac{\partial \sigma}{\partial z} \frac{\partial z}{\partial t} , \quad (2.21b)$$

where the subscripts are understood.

The model differential equations transformed into the (λ, ϕ, σ) coordinate system are presented below. It is useful to define

$$\omega = w - \frac{u}{a \cos \phi} \frac{\partial z}{\partial \lambda} - \frac{v}{a} \frac{\partial z}{\partial \phi} ; \quad (2.22a)$$

with this definition ω is the fluid velocity normal to the constant σ surfaces. That ω does not simply equal w results from the fact that the σ surfaces are not coincident in general with geopotential surfaces. We also define

$$q_\sigma = q_z - \frac{q_\lambda}{a \cos \phi} \frac{\partial z}{\partial \lambda} - \frac{q_\phi}{a} \frac{\partial z}{\partial \phi} ,$$

$$\gamma_\sigma = \gamma_z - \frac{\gamma_\lambda}{a \cos \phi} \frac{\partial z}{\partial \lambda} - \frac{\gamma_\phi}{a} \frac{\partial z}{\partial \phi} ,$$

$$\tau_{\sigma\lambda} = \tau_{z\lambda} - \frac{\tau_{\lambda\lambda}}{a \cos \phi} \frac{\partial z}{\partial \lambda} - \frac{\tau_{\phi\lambda}}{a} \frac{\partial z}{\partial \phi} ,$$

and

$$\tau_{\sigma\phi} = \tau_{z\phi} - \frac{\tau_{\lambda\phi}}{a \cos\phi} \frac{\partial z}{\partial \lambda} - \frac{\tau_{\phi\phi}}{a} \frac{\partial z}{\partial \phi} \quad (2.22b-e)$$

These quantities represent the sub-grid scale flux of heat, salt and momentum across constant σ surfaces.

The forecasting model differential equations transformed from (2.12) are:

$$\frac{\partial}{\partial \lambda} \left(u \frac{\partial z}{\partial \sigma} \right) + \frac{\partial}{\partial \phi} \left(v \cos\phi \frac{\partial z}{\partial \sigma} \right) + \frac{\partial}{\partial \sigma} (\omega a \cos\phi) = 0 \quad , \quad (2.23a)$$

$$\begin{aligned} \dot{T} - \frac{\partial T}{\partial \sigma} \frac{\partial \sigma}{\partial z} \dot{z} = & - \frac{1}{a \cos\phi} \frac{\partial \sigma}{\partial z} \left\{ \frac{\partial}{\partial \lambda} \left[(uT + q_{\lambda}) \frac{\partial z}{\partial \sigma} \right] + \frac{\partial}{\partial \phi} \left[(vT + q_{\phi}) \cos\phi \frac{\partial z}{\partial \sigma} \right] \right. \\ & \left. + \frac{\partial}{\partial \sigma} \left[(\omega T + q_{\sigma}) a \cos\phi \right] \right\} + \epsilon \quad , \quad (2.23b) \end{aligned}$$

$$\begin{aligned} \dot{S} - \frac{\partial S}{\partial \sigma} \frac{\partial \sigma}{\partial z} \dot{z} = & - \frac{1}{a \cos\phi} \frac{\partial \sigma}{\partial z} \left\{ \frac{\partial}{\partial \lambda} \left[(uS + \gamma_{\lambda}) \frac{\partial z}{\partial \sigma} \right] + \frac{\partial}{\partial \phi} \left[(vS + \gamma_{\phi}) \cos\phi \frac{\partial z}{\partial \sigma} \right] \right. \\ & \left. + \frac{\partial}{\partial \sigma} \left[(\omega S + \gamma_{\sigma}) a \cos\phi \right] \right\} \quad , \quad (2.23c) \end{aligned}$$

$$\begin{aligned} \dot{u} - \frac{\partial u}{\partial \sigma} \frac{\partial \sigma}{\partial z} \dot{z} = & - \frac{1}{a \cos\phi} \frac{\partial \sigma}{\partial z} \left\{ \frac{\partial}{\partial \lambda} \left[(uu - \tau_{\lambda\lambda}) \right] + \frac{\partial}{\partial \phi} \left[(vu - \tau_{\phi\lambda}) \cos\phi \frac{\partial z}{\partial \sigma} \right] \right. \\ & \left. + \frac{\partial}{\partial \sigma} \left[(\omega u - \tau_{\sigma\lambda}) a \cos\phi \right] \right\} + (vu - \tau_{\phi\lambda}) \frac{\tan\phi}{a} \\ & + vf - \frac{1}{\rho_0 a \cos\phi} \left[\frac{\partial p}{\partial \lambda} - \frac{\partial p}{\partial \sigma} \frac{\partial \sigma}{\partial z} \frac{\partial z}{\partial \lambda} \right] \quad , \quad (2.23d) \end{aligned}$$

$$\begin{aligned}
\dot{v} - \frac{\partial v}{\partial \sigma} \frac{\partial \sigma}{\partial z} \dot{z} = & - \frac{1}{a \cos \phi} \frac{\partial \sigma}{\partial z} \left\{ \frac{\partial}{\partial \lambda} \left[(uv - \tau_{\lambda\phi}) \frac{\partial z}{\partial \sigma} \right] + \frac{\partial}{\partial \phi} \left[(vv - \tau_{\phi\phi}) \cos \phi \frac{\partial z}{\partial \sigma} \right] \right. \\
& \left. + \frac{\partial}{\partial \sigma} \left[(\omega v - \tau_{\sigma\phi}) a \cos \phi \right] \right\} - (uu - \tau_{\lambda\lambda}) \frac{\tan \phi}{a} \\
& - \frac{1}{\rho_0 a} \left[\frac{\partial p}{\partial \phi} - \frac{\partial p}{\partial \sigma} \frac{\partial \sigma}{\partial z} \frac{\partial z}{\partial \phi} \right] \quad , \quad (2.23e)
\end{aligned}$$

and

$$\frac{\partial p}{\partial \sigma} = g \rho \frac{\partial z}{\partial \sigma} \quad . \quad (2.23f)$$

The time rate of change of z at constant λ, ϕ and σ which appears in the equations is determined from the analytic relation between z and σ . We differentiate (2.18) with respect to time to obtain

$$\dot{z} = \dot{z}_s \left[1 - \sigma \left(\frac{\delta + z - z_s}{\delta + z_b - z_s} \right) \right] \quad . \quad (2.24)$$

The rate of change of the surface elevation \dot{z}_s , is given by a surface boundary condition presented later.

The sub-grid scale heat fluxes given in (2.13) transform to

$$q_\lambda = - \frac{\beta_H K_H}{a \cos \phi} \left(\frac{\partial T}{\partial \lambda} - \frac{\partial T}{\partial \sigma} \frac{\partial \sigma}{\partial z} \frac{\partial z}{\partial \lambda} \right) \quad ,$$

$$q_\phi = - \frac{\beta_H K_H}{a} \left(\frac{\partial T}{\partial \phi} - \frac{\partial T}{\partial \sigma} \frac{\partial \sigma}{\partial z} \frac{\partial z}{\partial \phi} \right) \quad ,$$

and

$$q_z = - \beta_V K_V \frac{\partial T}{\partial \sigma} \frac{\partial \sigma}{\partial z} \quad . \quad (2.25a-c)$$

The salt fluxes γ_λ , γ_ϕ and γ_z transform similarly.

The components of the rate of strain tensor (2.14) transform to

$$e_{\lambda\lambda} = \frac{2}{a \cos \phi} \left(\frac{\partial u}{\partial \lambda} - \frac{\partial u}{\partial \sigma} \frac{\partial \sigma}{\partial z} \frac{\partial z}{\partial \lambda} - v \sin \phi \right) \quad ,$$

$$e_{\phi\lambda} = \frac{1}{a \cos \phi} \left[\frac{\partial v}{\partial \lambda} - \frac{\partial v}{\partial \sigma} \frac{\partial \sigma}{\partial z} \frac{\partial z}{\partial \lambda} + \left(\frac{\partial u}{\partial \phi} - \frac{\partial u}{\partial \sigma} \frac{\partial \sigma}{\partial z} \frac{\partial z}{\partial \phi} \right) \cos \phi \right. \\ \left. + u \sin \phi \right] \quad ,$$

$$e_{z\lambda} = \frac{\partial u}{\partial \sigma} \frac{\partial \sigma}{\partial z} \quad ,$$

$$e_{\phi\phi} = \frac{2}{a} \left(\frac{\partial v}{\partial \phi} - \frac{\partial v}{\partial \sigma} \frac{\partial \sigma}{\partial z} \frac{\partial z}{\partial \phi} \right) \quad ,$$

and

$$e_{z\phi} = \frac{\partial v}{\partial \sigma} \frac{\partial \sigma}{\partial z} \quad . \quad (2.26a-e)$$

The expressions for the sub-grid momentum fluxes are (2.15) with the above representation for the strain rates.

In the sigma coordinate system the horizontal diffusivity K_H is as given by (2.16) with the appropriate transformed expressions for $e_{\lambda\lambda}$, $e_{\phi\phi}$ and $e_{\phi\lambda}$. The vertical diffusivity defined by (2.8) becomes

$$K_V = \ell^2(z) \left[\left(\frac{\partial u}{\partial \sigma} \right)^2 + \left(\frac{\partial v}{\partial \sigma} \right)^2 \right]^{\frac{1}{2}} \frac{\partial \sigma}{\partial z} (1-R/R_c)^{3/2},$$

where

$$R = N^2 / \left\{ \left| \left(\frac{\partial u}{\partial \sigma} \right)^2 + \left(\frac{\partial v}{\partial \sigma} \right)^2 \right| \left(\frac{\partial \sigma}{\partial z} \right)^2 \right\},$$

$$R_c = 0.23,$$

and

$$N^2 = \frac{g}{\rho_0} \left[\left(\frac{\partial \rho}{\partial \sigma} \right)_{\lambda, \phi} \frac{\partial \sigma}{\partial z} - \rho g \left(\frac{\partial \rho}{\partial p} \right)_{TS} \right] \quad (2.27a-d)$$

We have made use of (2.12f) in obtaining (2.27d) from (2.8d).

The sigma-coordinate differential equation system which we have derived is completely specified with the incorporation of the equation of state. It is this system which will be approximated and solved numerically by our ocean forecasting computer model.

2.2 EQUATION OF STATE

There exist numerous formulations of an equation of state for seawater, of which the most widely known is probably that developed many years ago by Knudsen (Fofonoff, 1962). There is at present much activity in this field and recent emphasis has been on the development of thermodynamically consistent formulations, that is, on formulations which not only accurately represent the variation of density with temperature, salinity and pressure, but which also provide accurate sound speed predictions. Among the best of these recent formulations are two developed by Chen and Millero (1976, 1977). These formulas are of the general form

$$\rho = \rho_t / \left[1 + P / (K^0 + AP + BP^2) \right] , \quad (2.28a)$$

where ρ_t is the density at the *in situ* temperature and salinity but at a standard atmospheric pressure (1.013 bar), and P is the difference (in bars) between the actual and standard pressures

$$P = p - 1.013 \text{ (in bars)} \quad . \quad (2.28b)$$

The densities ρ and ρ_t are in units of gm/cm^3 . The quantities ρ_t , K^0 , A and B are given as functions of T and S .

In the first Chen and Millero formula (1977) the computation of these quantities involves 48 parameters and the state equation is valid over the range

$$5 \leq S \leq 40\text{‰} \quad ,$$

$$0 \leq P \leq 1000 \text{ bars,}$$

and

$$-2 \leq T \leq 40 \text{ }^\circ\text{C} \quad . \quad (2.29)$$

The second Chen and Millero formula (1977) is a simplification of the first for use in the open ocean involving 23 parameters. It is valid over the range

$$30 \leq S \leq 40\text{‰} \quad ,$$

$$0 \leq P \leq 1000 \text{ bars,}$$

and

$$-2 \leq T \leq 40 \text{ }^\circ\text{C} \quad . \quad (2.30)$$

The second Chen and Millero formula will be incorporated into our ocean forecasting code. The quantities p_t , K^O , A and B are given by

$$\begin{aligned} \rho_t = & 1.0281045 - 5.35633 \times 10^{-5} T - 6.78195 \times 10^{-6} T^2 \\ & + 7.0517 \times 10^{-8} T^3 - 8.4794 \times 10^{-10} T^4 + 5.057 \times 10^{-12} T^5 \\ & + (8.0792 \times 10^{-4} - 3.2481 \times 10^{-6} T + 6.423 \times 10^{-8} T^2 - 6.490 \times 10^{-10} T^3) \\ & \times (S - 35) + 2.045 \times 10^{-7} (S - 35)^2 \quad , \end{aligned}$$

$$K^{\circ} = 21585.72 + 132.5657 T - 2.0860 T^2 + 8.7648 \times 10^{-3} T^3 \\ + (56.928 - 0.2975 T) (S - 35) ,$$

$$A = 3.40075 - 7.6371 \times 10^{-3} T + 2.9651 \times 10^{-4} T^2 \\ (2.287 \times 10^{-3} - 3.255 \times 10^{-4} T) (S - 35) ,$$

and

$$B = 2.211 \times 10^{-5} . \quad (2.31)$$

With (2.28) we may now evaluate

$$\left(\frac{\partial \rho}{\partial p} \right)_{TS}$$

which appears in the definition of N^2 (2.27d). Differentiating (2.28) we obtain

$$\left(\frac{\partial \rho}{\partial p} \right)_{TS} = - \frac{\rho^2}{\rho_t} \frac{K^{\circ} - BP^2}{(K^{\circ} + AP + BP^2)} . \quad (2.32)$$

To conclude this section we note that Chen and Millero are at the time of this writing developing a new formulation under the guidance of The UNESCO/ICES/SCOR/IAPSO Joint Panel on Oceanographic Tables and Standards. This formulation, which will have the same general form as (2.28), is meant to be definitive and we will incorporate it into the computer code when it becomes available late in (1978).

2.3 MODIFICATIONS TO ALLEVIATE ROUNDING ERROR

Our ocean forecasting computer code will be programmed for the TI-ASC in single-precision arithmetic. The use of double precision increases the computation time for typical operations by a factor of about four. Since single precision arithmetic corresponds to roughly 6 to 8 significant figure accuracy, we must take care to alleviate as much as possible potential difficulties associated with round-off error. In this section we describe a modification to our ocean model equations which will help ensure that rounding error is kept to a minimum. As we encounter difficulties associated with round-off error in other aspects of our model, we will take appropriate steps to alleviate them.

2.3.1 Introduction of Reference State Density and Pressure

In the geostrophic approximation all of the terms in the horizontal momentum equations vanish except for the Coriolis and the pressure gradient terms, and, although in our ocean model we are not applying such an approximation, these terms will dominate the others. Their accurate calculation is thus very important. The Coriolis force term, being simply a product, poses no special difficulties; however, the pressure gradient term does. The pressure is obtained from the integration of (2.23f), and except near the surface, the pressure is very large compared with the surface pressure. The horizontal gradients of pressure which play a major role in the circulation dynamics are

very small compared to the vertical gradients so that round-off error associated with the pressure integration can pose serious difficulties.

In our (λ, ϕ, σ) coordinate system the round-off problem is especially acute. Consider the horizontal pressure force in the λ direction, from (2.23d)

$$- \frac{1}{\rho_0 a \cos \phi} \left[\left(\frac{\partial p}{\partial \lambda} \right)_\sigma - \frac{\partial p}{\partial \sigma} \frac{\partial \sigma}{\partial z} \left(\frac{\partial z}{\partial \lambda} \right)_\sigma \right] \quad . \quad (2.33)$$

Over much of the ocean $(\partial z / \partial \lambda)_\sigma$ will be small since the bottom topography changes slowly with λ as does the surface elevation z_s . Near the coasts, however, and at other locations where the depth variation is large, $(\partial z / \partial \lambda)_\sigma$ will not be small, and since $(\partial p / \partial \lambda)_\sigma$ then includes a significant vertical (z) component, the two terms in (2.33) are both very large. They are, however, almost equal so that their difference, which is the horizontal pressure gradient $(\partial p / \partial \lambda)_z$, is small. The subtraction of two large but almost equal numbers is the classic example of a situation in which round-off error can significantly degrade the accuracy of the result.

To reduce as much as possible the potential for significant rounding error, we modify the pressure with the introduction of a reference pressure given by

$$\frac{\partial p_r}{\partial z} = \rho_r(z)g \quad , \quad (2.34)$$

where $\rho_r(z)$ is a specified reference density distribution. A suitable reference density distribution might be obtained from a mean of oceanic observations. At $z = z_r$, we specify that p_r be a global mean atmospheric pressure p_{ra} . We subtract (2.34) from the hydrostatic relation (2.12f) in (λ, ϕ, z) coordinates and obtain

$$\frac{\partial \Pi}{\partial z} = g \left(\frac{\rho - \rho_r}{\rho_o} \right) \quad , \quad (2.35a)$$

where

$$\Pi = (p - p_r) / \rho_o \quad . \quad (2.35b)$$

Since p_r is a function of z only, we can replace p/ρ_o in the momentum equations in (λ, ϕ, z) coordinates by Π . When the equations, in terms of Π , are transformed into the (λ, ϕ, σ) coordinate system, the resulting equations are identical to (2.23) except that, in the horizontal momentum equations and the hydrostatic relation, p/ρ_o is replaced by Π . Thus the horizontal pressure gradient terms are

$$- \frac{1}{a \cos \phi} \left(\frac{\partial \Pi}{\partial \lambda} - \frac{\partial \Pi}{\partial \sigma} \frac{\partial \sigma}{\partial z} \frac{\partial z}{\partial \lambda} \right) \quad (2.36a)$$

in (2.23d) and

$$- \frac{1}{a} \left(\frac{\partial \Pi}{\partial \phi} - \frac{\partial \Pi}{\partial \sigma} \frac{\partial \sigma}{\partial z} \frac{\partial z}{\partial \phi} \right) \quad (2.36b)$$

in (2.23e). The hydrostatic relation becomes

$$\frac{\partial \Pi}{\partial \sigma} = g \left(\frac{\rho - \rho_r}{\rho_o} \right) \frac{\partial z}{\partial \sigma} \quad . \quad (2.37)$$

2.4 USER-SPECIFIED POLES

A feature which will be incorporated into the ocean forecasting model is an option for user-specified location of the coordinate system poles $\phi = \pm 90^\circ$. The user-specified pole feature will be useful in both whole-ocean and limited region forecasts since with its application λ and ϕ coordinate lines can be aligned with major features of the ocean region under consideration. This possibility is especially attractive in conjunction with the variable-mesh-width finite-difference scheme described later in this report.

A second application of the user-specified pole feature might be to limited-area forecasts in high latitude regions. Since the "equator" of the coordinate system, $\phi = 0$, can be specified as passing through any point on the earth's surface, a λ - ϕ mesh system for a limited region which is nearly rectangular in distance is possible anywhere. An example of the utility of this feature is that our model can be applied directly to forecasts of the North Polar Sea without the grid-related numerical difficulties generally encountered near the geographic poles.

A third application of the user-specified pole feature will be to very large region forecasts (hemispherical or global) which include the polar regions. In these cases, the coordinate system poles can be located over land masses so that, as mentioned above, numerical difficulties associated with flow near the poles are avoided. Two pairs of overland antipodal locations which might be suitable for global forecasts are $30^\circ\text{N } 110^\circ\text{E} - 30^\circ\text{S } 70^\circ\text{W}$ (Western China-Argentina) and $75^\circ\text{N } 40^\circ\text{W} - 75^\circ\text{S } 140^\circ\text{E}$ (Greenland-Antarctica).

The variable-pole capability will require a simple data transfer subroutine to convert data reported at conventional longitude-latitude points to the model λ - ϕ coordinates. If (λ_p, ϕ_p) is the desired geographic location of the "north" pole in terms of conventional longitude and latitude, then a new longitude-latitude system is given by

$$\lambda^* = \tan^{-1} \left[\frac{\cos \phi \sin(\lambda_p - \lambda)}{\sin \phi \cos \phi_p - \cos \phi \sin \phi_p \cos(\lambda_p - \lambda)} \right], \quad (2.38a)$$

and

$$\phi^* = \sin^{-1} [\cos \phi \cos \phi_p \cos(\lambda_p - \lambda) + \sin \phi \sin \phi_p] \quad (2.38b)$$

where we have defined

$$\lambda^* = 0 \text{ at } \lambda = \lambda_p - \pi.$$

The new coordinate system has one of its poles at (λ_p, ϕ_p) and its zero meridian passes through the geographic North Pole.

We emphasize that the computer code input and output will always be in terms of conventional longitude and latitude. The Coriolis parameter f must, of course, also be determined from the conventional latitude.

2.5 BOUNDARY CONDITIONS

In this section we present appropriate boundary conditions for the ocean forecasting model equations described in the previous section. We remind the reader that the lateral boundaries are located at $\lambda_W, \lambda_E, \phi_S$ and ϕ_N , and that the ocean surface and the bottom are located at $\sigma = 0$ and $\sigma = 1$, respectively. We present ocean surface and bottom conditions, and three types of lateral boundary conditions: no-flux, flux, and periodic in longitude

2.5.1 Ocean Surface Conditions

In this section we describe a set of ocean surface boundary conditions. More sophisticated parameterizations of the transport of heat and momentum across the ocean surface and of the effects of evaporation and precipitation may be implemented as the forecasting model is developed. In what follows the subscript "s" will be used to denote quantities evaluated at the surface.

At the ocean surface we require

$$\frac{D}{Dt}(z-z_s) = F_s \quad , \quad (2.39a)$$

where F_s is the net volume flux of fresh water at the surface due to precipitation and evaporation (precipitation makes a positive contribution to F_s). In terms of the fluid velocity in the σ direction defined in (2.22a) we have

$$\dot{z}_s = \omega - F_s \quad . \quad (2.39b)$$

Equation (2.39b) will be solved numerically in time for z_s as part of the overall solution process.

To obtain a surface condition for T we assume that either the surface water temperature or the heat flux through the surface, q_s , is specified. The surface heat flux might be expressed in terms of the surface temperature and salinity. When the surface temperature T_s is specified, the boundary condition on T is obviously

$$T = T_s(\lambda, \phi, t) \quad . \quad (2.40)$$

The heat flux through the surface is specified by

$$q_{\sigma, s} = q_s(\lambda, \phi, t, T_s, S_s) \quad . \quad (2.41)$$

We require that there be no flux of salt through the ocean surface. To satisfy this condition we specify

$$\gamma_{\sigma, s} = - F_s S_s \quad . \quad (2.42)$$

We will demonstrate that (2.42) is the appropriate condition for zero surface flux in Section 2.6 (see equations (2.54) and related discussion).

The surface windstress will be estimated from the near surface wind velocity using the simple formulas

$$\tau_{\sigma\lambda,s} = - C_D u_a \frac{\rho_a}{\rho_0} (u_a^2 + v_a^2)^{\frac{1}{2}},$$

and

$$\tau_{\sigma\phi,s} = - C_D v_a \frac{\rho_a}{\rho_0} (u_a^2 + v_a^2)^{\frac{1}{2}}, \quad (2.43a,b)$$

where C_D is an appropriate friction coefficient, u_a and v_a are the longitudinal and latitudinal components of the surface wind velocity, and ρ_a is a mean air density. Typical values of C_D are about 3×10^{-3} (Sverdrup, Johnson and Fleming, 1942).

Finally, we require that at the surface the pressure p equals the specified atmospheric pressure $p_a(\lambda, \phi, t)$. In terms of the modified pressure, we require

$$\Pi_s = [p_a - p_r(z_s)] / \rho_0 \quad (2.43c)$$

2.5.2 Ocean Bottom Conditions

In this section we present a set of ocean bottom boundary conditions. Subscript "b" will be used to refer to quantities evaluated at the bottom. We assume that the model predictions will not be very sensitive to the imposed

bottom boundary conditions so we are permitted some flexibility in their specification. Should any of the approximate conditions presented here prove inadequate, it will be suitably modified.

The condition that fluid does not cross the ocean bottom is given by

$$\frac{D}{Dt}(z-z_b) = 0 \quad . \quad (2.44a)$$

Since $\dot{z}_b = 0$ we have, in our (λ, ϕ, σ) coordinate system,

$$\omega_b = 0 \quad , \quad (2.44b)$$

which will be used to initialize the vertical integration of (2.23a) for ω .

The bottom condition on T is obtained from the condition that there be no bottom heat flux into the ocean, that is,

$$q_{\sigma,b} = 0 \quad . \quad (2.45)$$

Similarly we require

$$\gamma_{\sigma,b} = 0 \quad , \quad (2.46)$$

as the bottom boundary condition on the salinity.

Finally, conditions are required for the u and v velocity components. We propose

$$u + \frac{\delta z}{d} \frac{\partial u}{\partial \sigma} \delta \sigma = 0 \quad ,$$

and

$$v + \frac{\delta z}{d} \frac{\partial v}{\partial \sigma} \delta \sigma = 0 \quad ,$$

where

$$d = \left[\frac{u^2 + v^2}{N^2 + f^2} \right]^{\frac{1}{2}} \quad , \quad (2.47a-c)$$

δz is the distance (in z) between the bottom and the first finite-difference mesh point above the bottom, and $\delta \sigma$ is that grid spacing in terms of σ . The quantity d is a bottom-layer thickness length scale. As either N or the Coriolis parameter increase, d decreases corresponding to the suppression of vertical transport by buoyancy forces in the former case and to the occurrence of a thin Ekman layer in the latter.

The meaning of (2.47) is made clear by the consideration of two limiting cases, $\delta z \gg d$ and $\delta z \ll d$. When $\delta z \gg d$, we have no hope of resolving the bottom boundary layer so a no-slip bottom condition cannot be applied. In this case (2.47a) and (2.47b) become

$$\frac{\partial u}{\partial \sigma} = 0 \quad \text{and} \quad \frac{\partial v}{\partial \sigma} = 0 \quad .$$

When $\delta z \ll d$, we do expect to be able to resolve the bottom layer. In this case (2.47a) and (2.47b) become

$$u = 0 \quad \text{and} \quad v = 0 \quad ,$$

which is just the no-slip condition. The signs in (2.47a,b) have been chosen so that in the intermediate case the velocity gradient has the correct sign.

2.5.3 No-Flux Lateral Boundary Conditions

No-flux lateral boundary conditions are unphysical except at boundaries located over land areas. Such will be the case in whole ocean forecasts where the boundaries will be located over, but near the coasts of, the surrounding land areas.

For the heat, salt, mass and momentum fluxes to vanish at a longitudinal boundary, we require

$$q_{\lambda} = 0 \quad ,$$

$$\gamma_{\lambda} = 0 \quad ,$$

and

$$u = 0 \quad .$$

We also require a condition on v , the velocity component parallel to the boundary, and we specify

$$\frac{\partial v}{\partial \lambda} = 0 \quad . \quad (2.48a-d)$$

No-flux conditions at a latitudinal boundary, ϕ_S or ϕ_N , are specified in similar fashion as

$$q_\phi = 0 \quad ,$$

$$\gamma_\phi = 0 \quad ,$$

$$v = 0 \quad ,$$

and

$$\frac{\partial u}{\partial \phi} = 0 \quad . \quad (2.49a-d)$$

2.5.4 Flux Lateral Boundary Conditions

Flux lateral boundary conditions will be applied in limited region forecasts when T , S , u , v and z_s are specified along the region boundaries. This will typically be the case when high-resolution numerical forecasts for limited regions are imbedded into lower resolution forecasts for larger regions. In such cases careful interpolation procedures must be used in the generation of lateral boundary conditions for the high resolution computation from the lower resolution predictions.

Along inflow boundaries (where the velocity normal to the boundary is directed into the region), we have

$$T, S, u, v \text{ and } z_s \text{ specified.} \quad (2.50)$$

Conditions (2.50) will be obtained by interpolation from a large region, low resolution forecast.

Along outflow boundaries we require that the second spatial derivatives of T and S normal to the boundary be zero, and the velocity component normal to the boundary be specified. We require the second derivative of the velocity component parallel to the boundary be zero, and z_s be specified.

Along the longitudinal boundary the outflow conditions are

$$\frac{\partial^2 T}{\partial \lambda^2} = 0 \quad ,$$

$$\frac{\partial^2 S}{\partial \lambda^2} = 0 \quad ,$$

$$u \text{ specified} \quad ,$$

$$\frac{\partial^2 v}{\partial \lambda^2} = 0$$

$$\text{and } z_s \text{ specified} \quad . \quad (2.51a-e)$$

Along a latitudinal boundary the outflow conditions are

$$\frac{\partial^2 T}{\partial \phi^2} = 0 \quad ,$$

$$\frac{\partial^2 S}{\partial \phi^2} = 0 \quad ,$$

v specified ,

$$\frac{\partial^2 u}{\partial \phi^2} = 0$$

and z_s specified . (2.52a-e)

We apply second-derivative outflow conditions since specification of the quantities themselves will in general lead to numerical problems associated with the development of a narrow "boundary layer" at the boundary (see the discussion of "wiggles" in Roache, 1972). The velocity component normal to the boundary can be specified, however, since the development of a "boundary layer" for this quantity is prevented by the action of the pressure gradient normal to the boundary.

We add a constraint to our interpolation procedure for the velocity component normal to the boundaries. We require the appropriate numerical representations of the net volume flux into the limited region be the same for both the low and high resolution forecasts. This is essential to ensure a consistent low resolution forecast.

2.5.5 Periodicity Conditions in Longitude

Periodicity conditions in longitude will be appropriate for hemispherical and global forecasts. In terms of our boundaries λ_W and λ_E , we simply set

$$\lambda_W = 0^\circ ,$$

$$\lambda_E = 360^\circ \text{ (or equivalently, } 2\pi) ,$$

$$z(\lambda_E) = z(\lambda_W) ,$$

$$T(\lambda_E) = T(\lambda_W) ,$$

$$S(\lambda_E) = S(\lambda_W) ,$$

$$u(\lambda_E) = u(\lambda_W) ,$$

and

$$v(\lambda_E) = v(\lambda_W) \quad \cdot \quad (2.53a-g)$$

2.6 INTEGRAL PROPERTIES OF THE MODEL EQUATIONS

In this section we discuss integral properties of the model differential equations (2.23). These properties provide guidance in the development of the numerical representation of the equations by finite differences.

Equations (2.23b) and (2.23c) represent the conservation of heat and salt. It is easy to integrate them over the forecast region $\lambda_W \leq \lambda \leq \lambda_E$, $\phi_S \leq \phi \leq \phi_N$ and $0 \leq \sigma \leq 1$. We make use of the surface and bottom conditions (2.39), (2.44), (2.45) and (2.46) to obtain

$$\begin{aligned} \frac{\partial}{\partial \tau} \int_V T dV = & - \int_{A_L} (\underline{v}T + q) \cdot \hat{n}_L dA_L + \int_{A_S} (F_S T_S + q_{\sigma, S}) dA_S \\ & + \int_V \epsilon dV \end{aligned} \quad (2.54a)$$

and

$$\begin{aligned} \frac{\partial}{\partial \tau} \int_V S dV = & - \int_{A_L} (\underline{v}S + \gamma) \cdot \hat{n}_L dA_L + \int_{A_S} (F_S S_S + \gamma_{\sigma, S}) dA_S \end{aligned} \quad (2.54b)$$

where

$$dV = a^2 \cos \phi d\lambda d\phi \frac{\partial z}{\partial \sigma} d\sigma$$

is the element of volume, A_L is the surface area of the lateral boundaries, \hat{n}_L is the local unit normal to the

lateral boundary (directed outward), A_S is the ocean region surface area and

$$dA_S = a^2 \cos\phi d\lambda d\phi .$$

Equations (2.54) demonstrate that the rates of change of TdV and SdV integrated over the forecast region are equal to the appropriate net fluxes into the region through its boundaries, plus the volume integrals of any sources within the region. We see that with the surface salinity condition (2.42), the surface salt flux is zero.

We can also derive a second property of (2.23b) and (2.23c). We neglect the sub-grid fluxes of heat and salt and the source term ϵ . We multiply (2.23b) by T , (2.23c) by S and integrate over the forecast region. We make use of continuity (2.23a) and the kinematic conditions at the surface and bottom, (2.39) and (2.44), and we obtain

$$\frac{\partial}{\partial t} \int_V \frac{1}{2} T^2 dV = - \int_{A_L} \frac{1}{2} T^2 \underline{u} \cdot \hat{n}_L dA_L + \int_{A_S} \frac{1}{2} T^2 F_S dA_S ,$$

(2.55a)

and

$$\frac{\partial}{\partial t} \int_V \frac{1}{2} S^2 dV = - \int_{A_L} \frac{1}{2} S^2 \underline{u} \cdot \hat{n}_L dA_L + \int_{A_S} \frac{1}{2} S^2 F_S dA_S .$$

(2.55b)

Equations (2.55) demonstrate that under advection the rates of change of the volume integrals of T^2 and S^2 simply equal the fluxes of T^2 and S^2 through the region boundaries.

This property is especially useful in the development of a finite-difference scheme which is not prone to "non-linear instability".

Finally, we may derive an integral property of the horizontal momentum equations (2.23d) and (2.23e). We use the modified pressure terms (2.36), neglect the sub-grid stresses, and multiply (2.23d) by u and (2.23e) by v . We add the resulting equations and integrate over the forecast region V . We make use of continuity (2.23a), (2.39) and (2.44), and we obtain

$$\begin{aligned} \frac{\partial}{\partial t} \int_V \frac{1}{2}(u^2+v^2) dV &= \int_V w \frac{\partial \Pi}{\partial \sigma} \frac{\partial \sigma}{\partial z} dV \\ &+ \int_{A_S} \left[\Pi_S (\dot{z}_S + F_S) + \frac{1}{2}(u^2+v^2) F_S \right] dA_S \\ &- \int_{A_L} \left[\Pi + \frac{1}{2}(u^2+v^2) \right] \underline{u} \cdot \hat{n}_L dA_L \quad . \end{aligned} \quad (2.56)$$

Equation (2.56) shows that with the neglect of the sub-grid fluxes, the rate of change of the total system horizontal kinetic energy is equal to the work done against the buoyancy forces, plus the energy flux and pressure work at the boundaries. The energy lost doing work against the buoyancy forces is added to the potential energy of the system. We will require that our finite-difference representation of the horizontal momentum equations satisfies a finite-difference representation of (2.56).

2.7 OCEAN FORECASTING MODEL SUMMARY

Since we have presented a great deal of material in this section, it is probably useful to conclude it with a summary of the ocean forecasting model equations which we have developed. We present such a summary in Table 2.1.

The extent of the forecast region is given by (2.17), and we have introduced a transformed vertical coordinate σ in (2.18). The model differential equations are (2.23) but expressed in terms of the modified pressure Π defined by (2.35), with the lateral pressure gradients given by (2.36) and the hydrostatic relation by (2.37). The time rate of change of z at constant σ is given by (2.24) in terms of z_s . The mean velocity and the sub-grid fluxes in the σ direction are defined in (2.22), and the sub-grid heat and salt fluxes (in the λ, ϕ and z directions) are given by (2.25). The sub-grid momentum fluxes are expressed in (2.15) with the components of the rate-of-strain tensor given by (2.26). The horizontal sub-grid diffusivity is given by (2.16) with the appropriate expressions for $e_{\lambda\lambda}$, $e_{\phi\phi}$ and $e_{\phi\lambda}$ from (2.26). The vertical sub-grid diffusivity is given by (2.27) with N given by (2.32). The equation of state is (2.29).

An option for user specified poles is described in Section 2.4, and expressions for λ and ϕ in the coordinate system with poles located other than at $\phi = \pm 90^\circ$ are given by (2.38).

TABLE 2.1 SUMMARY OF OCEAN FORECASTING MODEL EQUATIONS

MODEL COMPONENT	EQUATION REFERENCE NUMBER
Forecast Region	(2.17)
Transformed Vertical Coordinate	(2.18)
Modified Pressure Definition (Π)	(2.35)
Model Differential Equations and Π Modifications	(2.23), (2.36) and (2.37)
Time Rate of Change of z	(2.24)
Mean Velocity and Fluxes in σ Direction	(2.22)
Sub-Grid Heat and Salt Fluxes (λ, ϕ, z)	(2.25)
Rate-of-Strain Tensor	(2.26)
Sub-Grid Momentum Fluxes	(2.15) and (2.26)
Horizontal Sub-Grid Diffusivity	(2.16) and (2.26)
Vertical Sub-Grid Diffusivity	(2.27) and (2.32)
Equation of State	(2.29) and (2.31)
Variable Poles	(2.38)
Ocean Surface Boundary Conditions	(2.39) through (2.43)
Ocean Bottom Boundary Conditions	(2.44) through (2.47)
No-Flux Lateral Boundary Conditions	(2.48) and (2.49)
Flux Lateral Boundary Conditions	(2.50) through (2.52)
Periodic Conditions in Longitude	(2.53)

Ocean surface boundary conditions are given by (2.39) through (2.43), and bottom conditions by (2.44) through (2.47). No-flux lateral conditions are given by (2.48) and (2.49). Flux conditions are given in (2.50) through (2.52), and periodicity in longitude by (2.53).

The reader will probably recognize that we have left several loose. These will be tied down during the second phase of model development. We will develop a relationship based on experimental data between β_V and the local Richardson number. We will incorporate a suitable model for the absorption of solar radiation using the extinction curve of Jerlov (1961) or more recent work. We will develop an appropriate turbulent length scale specification technique, probably by relating it to a model predicted estimate of the mixed-layer depth. We will incorporate a parameterization of surface evaporation, including evaporative heat flux.

Section 3

SPATIAL FINITE-DIFFERENCE REPRESENTATION

We obtain finite-difference representations of the ocean model equations following a "box" approach similar to that described by Bryan (1966). The difference equations are constructed to be second-order accurate in the mesh spacing, and to have four important conservation properties. The numerical scheme we have developed ensures in the absence of temporal differencing errors, that

1. the time rate of change of a representation of the volume integrated heat and salt within the computational region is exactly equal to the net heat and salt flux through the region boundaries;
2. the time rate of change of representations of the volume integrals of the quadratic quantities T^2 and S^2 , are zero under the action of the advection terms;
3. the time rate of change of a representation of the volume integrated horizontal kinetic energy $(u^2+v^2)/2$ is zero under the action of the advection terms; and
4. the rate of increase of the representation of the volume integrated kinetic energy under the action of the horizontal pressure gradient is equal to a natural representation of the rate of work done by buoyancy forces, plus the rate of pressure work at the boundaries.

The first of these properties is the finite-difference equivalent of (2.54), the second is the equivalent of (2.55), and the third and fourth are the equivalent of (2.56).

By requiring that positive-definite quantities remain bounded, the second and third of these four properties free the scheme from the problems associated with "non-linear instability". An important corollary of the third and fourth properties is that the rate of change of the total horizontal kinetic energy is exactly equal to the work done by buoyancy forces and the surface pressure (in the absence of turbulent stresses and boundary fluxes) since the Coriolis force and the "geometry" terms $v \tan \phi / a$ and $-u^2 \tan \phi / a$ in (2.23d and e) do no net work.

3.1 THE FINITE-DIFFERENCE GRID SYSTEM

3.1.1 The Grid System

We overlay the solution domain

$$\lambda_W \leq \lambda \leq \lambda_E \quad ,$$

$$\phi_S \leq \phi \leq \phi_N \quad ,$$

and

$$0 \leq \sigma \leq 1 \quad ,$$

with a finite-difference grid system denoted by the discrete values $\lambda_{i+\frac{1}{2}}$, $\phi_{j+\frac{1}{2}}$, σ_k where

$$i = 1, 2, \dots, I \quad ,$$

$$j = 1, 2, \dots, J \quad ,$$

and

$$k = 2, 3, \dots, K \quad .$$

The grid system is arranged in the lateral plane (see Figure 1) such that the lateral boundaries are located halfway between mesh lines, so that

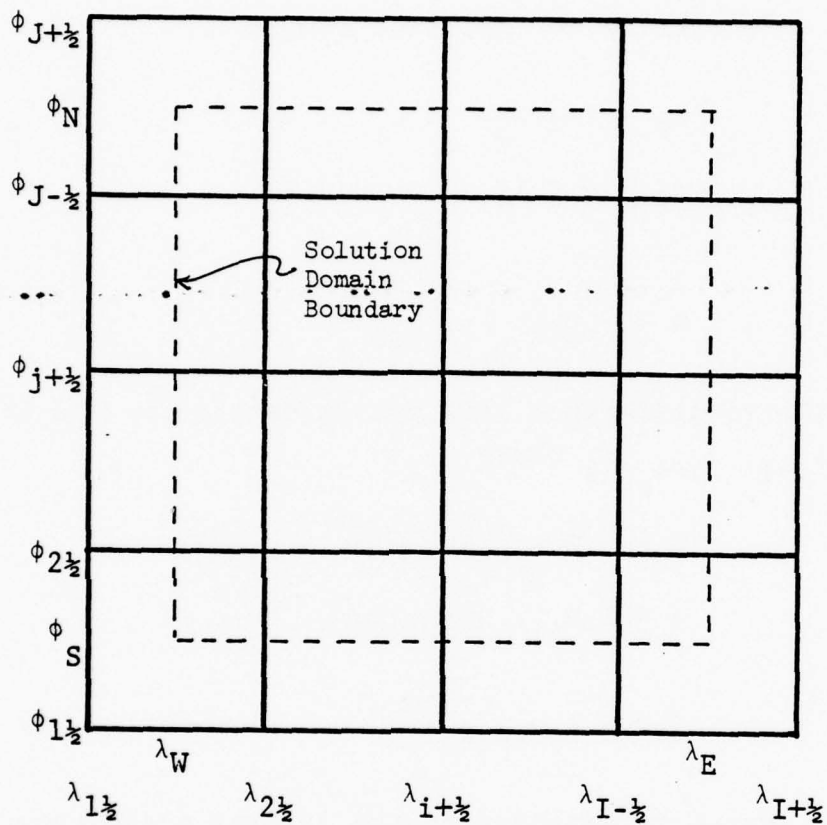


Figure 1. Basic Finite-Difference Grid System in Lateral Plane

$$\lambda_W = \frac{1}{2}(\lambda_{2\frac{1}{2}} + \lambda_{1\frac{1}{2}}) \quad ,$$

$$\lambda_E = \frac{1}{2}(\lambda_{I+\frac{1}{2}} + \lambda_{I-\frac{1}{2}}) \quad ,$$

$$\phi_S = \frac{1}{2}(\phi_{2\frac{1}{2}} + \phi_{1\frac{1}{2}}) \quad ,$$

and

$$\phi_N = \frac{1}{2}(\phi_{J+\frac{1}{2}} + \phi_{J-\frac{1}{2}}) \quad . \quad (3.1a-d)$$

The mesh lines at $\lambda_{1\frac{1}{2}}$, $\lambda_{I+\frac{1}{2}}$, $\phi_{1\frac{1}{2}}$, and $\phi_{J+\frac{1}{2}}$ thus fall outside the domain; these exterior mesh lines will be useful in the application of boundary conditions as described in a following section. We also specify that

$$\sigma_2 = 0$$

and

$$\sigma_K = 1 \quad (3.1e,f)$$

so that σ_2 is coincident with the upper surface and σ_K , the lower. We note that the index "2" is assigned to k at the upper boundary instead of "1" so that when additional grid points are defined above the surface to facilitate the application of boundary conditions, as described in a following section, the index system will be directly FORTRAN compatible (FORTRAN indices must be integers greater than zero).

We allow the horizontal grid spacings, $\lambda_{i+\frac{1}{2}} - \lambda_{i-\frac{1}{2}}$ and $\phi_{j+\frac{1}{2}} - \phi_{j-\frac{1}{2}}$, to vary, but their variation must be smooth to insure second-order accuracy. We restrict the grid spacing in σ , $\sigma_{k+1} - \sigma_k$, to be uniform.

In order to simplify the presentation and manipulation of the finite-difference equations, we introduce the two-point averaging and differencing operators

$$\bar{\zeta}^i = (\zeta_{i+\frac{1}{2}} + \zeta_{i-\frac{1}{2}})/2$$

and

$$\delta_i \zeta = \zeta_{i+\frac{1}{2}} - \zeta_{i-\frac{1}{2}} \quad (3.2a, b)$$

Similar operators are defined for averages and differences in j and k . The operators commute with each other in all three indices; for example

$$\delta_i \bar{\zeta}^j = \overline{\delta_i \zeta}^j$$

The commutability of the averaging operators allows us to write, unambiguously

$$\bar{\zeta}^{ik} = \overline{\bar{\zeta}^i}^k = \overline{\bar{\zeta}^k}^i$$

so that an overbar with more than one associated superscript represents the averaging operator in each of those superscripts applied in any convenient order.

Since λ , ϕ and σ are defined, in the finite-difference approximation with the discrete values $\lambda_{i+\frac{1}{2}}$, $\phi_{j+\frac{1}{2}}$ and σ_k only, the subscripts of these quantities will henceforth be neglected; and since the averaging and differencing operators may be applied to these quantities in meaningful fashion only in i , j and k , respectively, the sub and superscripts in these operations will also be neglected. Our neglect of these indices simplifies the presentation without

any loss of clarity. With these conventions, the difference grid spacings are denoted by $\delta\lambda$, $\delta\phi$ and $\delta\sigma$, where $\delta\lambda$ and $\delta\phi$ will in general vary with position.

In order to represent derivatives by finite-differences with a minimum of truncation error, some of the dependent variables will be located on mesh lines staggered with respect to the mesh system described above. We define a staggered set of mesh lines at locations midway between the λ , ϕ , and σ lines. We denote the staggered system by $\bar{\lambda}$, $\bar{\phi}$ and $\bar{\sigma}$, following our definition of the two-point averaging operator, and we associate with the staggered system the indices i , j and $k+\frac{1}{2}$. As a result of our definition of the system, staggered grid lines coincide with the lateral boundaries of the region, that is,

$$\lambda_W = \bar{\lambda}_2 \quad ,$$

$$\lambda_E = \bar{\lambda}_I \quad ,$$

$$\phi_S = \bar{\phi}_2 \quad ,$$

and

$$\phi_N = \bar{\phi}_J \quad . \quad (3.3a-d)$$

The index "2" is assigned to λ and ϕ at the West and South boundaries to facilitate the application in the FORTRAN code of boundary conditions there.

The latitude functions $\cos \phi$ and $\sin \phi$ are defined only at the $\bar{\phi}$ latitudes. In the finite-difference equations presented in the following sections

$$c \equiv \cos \bar{\phi}$$

and

$$s \equiv \sin \bar{\phi} \quad , \quad (3.4a,b)$$

and since two-point averages of c and s are meaningful only in j , we neglect the j superscript and represent these averages as \bar{c} and \bar{s} . The Coriolis parameter f will be defined at ϕ latitudes.

3.1.2 Arrangement of Dependent Variables

The dependent variables are arranged as shown in Figure 2. The temperature and salinity, T and S , are defined at $i, j, k+\frac{1}{2}$, that is, at the intersections of mesh lines $\bar{\lambda}$, $\bar{\phi}$ and $\bar{\sigma}$, and the pressure quantity Π is defined directly above the T-S point, at i, j, k . Thus, T, S and Π are defined on the lateral boundaries $\bar{\lambda}_2, \bar{\lambda}_1, \bar{\phi}_2$, and $\bar{\phi}_J$. The horizontal velocity components u and v are defined at $i+\frac{1}{2}, j+\frac{1}{2}, k+\frac{1}{2}$, that is, at the intersections of mesh lines $\lambda, \phi, \bar{\sigma}$, and the depth z is defined directly above the $u-v$ point, at $i+\frac{1}{2}, j+\frac{1}{2}, k$. Although it does not appear explicitly in the finite-difference equations, the vertical velocity is most conveniently computed at the Π -points.

Several factors are responsible for our choice of grid arrangement. Since the differential equations for T and S are identical, except for the source term ϵ , it is convenient to locate T and S at the same mesh point. Then, since the horizontal velocity components u and v are used in the computation of T and S fluxes, it is convenient to locate them at the same vertical (σ) level as T and S . The boundary

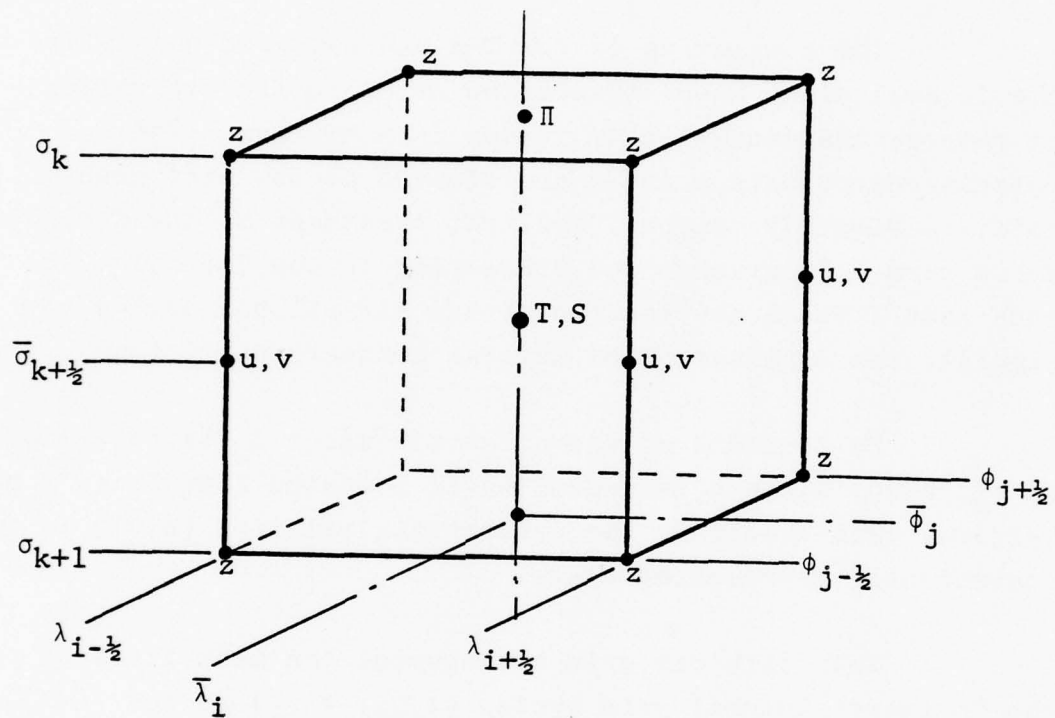


Figure 2. Arrangement of Variables and T-S Grid Cell.

conditions on T, S, u and v at the ocean surface are derivative conditions, except for those cases in which T might be specified at the surface, and it is numerically convenient to locate T, S, u and v at vertical half-mesh points $\bar{\sigma}$.

The staggering of the T-S and u-v grid points in the lateral plane keeps truncation error in the evaluation of temperature and salinity fluxes to a minimum. The velocity components u and v are located at the same mesh point to simplify temporal implicit treatment of the Coriolis force term. We arrange the staggering in the lateral plane such that T and S are located at the lateral boundaries to simplify the application of lateral boundary conditions.

We locate Π at the σ_k levels since Π_s is specified at σ_2 ; also, since ρ is conveniently computed from T and S at vertical grid levels $\bar{\sigma}$, the hydrostatic relation (2.37) is conveniently represented there.

That with our grid arrangement the mesh lines of the "primary" lateral grid system $(\lambda_{i+\frac{1}{2}}, \phi_{j+\frac{1}{2}})$ do not coincide with the lateral boundaries, while mesh lines of the averaged system $(\bar{\lambda}_i, \bar{\phi}_j)$ do coincide, resulted from our desire that the T-S points be located halfway between the u-v points and that T-S points be located on the lateral boundaries. With this grid arrangement the cross-sectional area normal to the vertical of a T-S grid cell is given by $a^2 c \delta \lambda \delta \phi$. In our difference scheme this area is the fundamental lateral cell area.

In order to incorporate bottom topography and to allow the computation of the lateral fluxes as accurately as possible, we chose to locate z vertically between the u-v

points at $i+\frac{1}{2}$, $j+\frac{1}{2}$, k . In our difference scheme the lateral volume fluxes, which are responsible for the mean lateral heat, salt and momentum fluxes, are computed at the u-v points and are proportional to the appropriate lateral velocity components and the cross-sectional cell areas normal to those components. Thus, the fluxes are most accurately computed when the cross-sectional area is most accurately specified at the velocity locations. Such is the case when z is located as we have proposed. To make clear the advantages of locating z above the u-v points, consider the simple example of a narrow isthmus coinciding with the meridian λ_L . Suppose we adjust our grid system so that $\lambda_L = \lambda_{i+\frac{1}{2}}$, along which both u and z are defined, then since $z_b - z_s$ will be very small along λ_L , the volume flux across the isthmus will be very small, as it should be. Consider now, z at a second likely location, the Π points. Locating z at the Π points is attractive since z at those points is required for the numerical treatment of the hydrostatic relation. However, since the computation of the volume flux in the λ direction requires z at the u-v points and since z at the u-v points would be computed from two-point averages of z in i and j , a negligibly small flux across the isthmus could be ensured only if it were two grid points wide. Adjusting the grid so that $\lambda_L = \bar{\lambda}_i$ will not help.

Finally, we note that the surface water flux F_s will be defined at $k=2$ at the $\bar{\lambda}_i$, $\bar{\phi}_j$ grid points since at these locations the surface condition on z_s will be applied. The heat source ϵ will be defined at the T-S points for obvious reasons.

3.2 THE FINITE-DIFFERENCE EQUATIONS

We obtain a finite-difference representation of the model differential equations (2.23) with (2.36) and (2.37) following a "box" approach of the sort described by Bryan (1966). In essence, we conceive of grid cells located about each grid point. The dependent variable defined at the grid point is assumed to represent a kind of average over the grid cell, and the rate of change of the variable times the volume of the cell is set equal to the net flux of that quantity across the cell surfaces, plus the rates of change due to source terms or body forces which are evaluated at the cell center. Our formulation is complicated by the fact that our cell volumes in (λ, ϕ, z) space vary with time.

In what follows, we let

$$\alpha_{\lambda} = a\delta\bar{\phi}\delta_k z \quad ,$$

$$\alpha_{\phi} = a\bar{c}\delta\bar{\lambda}\delta_k z \quad ,$$

$$\alpha_z = a^2 c\delta\lambda\delta\phi$$

and

$$V = \alpha_z \delta_k \bar{z}^{ij} \quad . \quad (3.5a-d)$$

The quantities $a\delta\lambda$ and $a\delta\phi$ represent the lateral dimensions of the T-S grid-cell centered at $i, j, k+\frac{1}{2}$ (see Figure 2) so that α_z is the cross-sectional cell area normal to the vertical, and V is the volume of the cell. The quantities α_{λ} and α_{ϕ} are cross-sectional areas of the u-v cell centered at $i+\frac{1}{2}, j+\frac{1}{2}, k+\frac{1}{2}$ normal to the λ and ϕ directions (Figure 3).

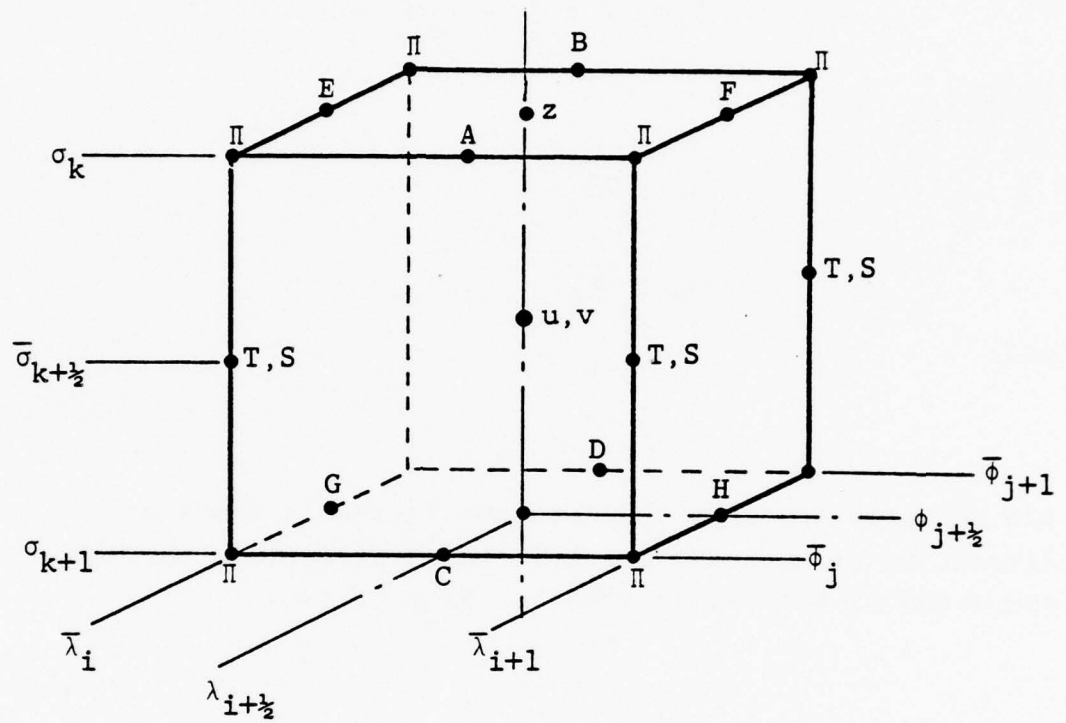


Figure 3. The u-v Grid Cell. The areas of faces ABCD and EFGH are represented by α_λ and α_ϕ .

3.2.1 The Continuity Equation

We represent the continuity equation (2.23a) at T-S grid points $(i, j, k+\frac{1}{2})$ by

$$\delta_i G_\lambda + \delta_j G_\phi + \delta_k G_\sigma = 0 \quad ,$$

where

$$G_\lambda = \overline{u\alpha}_\lambda^j \quad ,$$

$$G_\phi = \overline{v\alpha}_\phi^i \quad ,$$

and

$$G_\sigma = \omega\alpha_z \quad (3.6a-d)$$

are the grid resolved scale volume fluxes in the λ and ϕ directions at constant z and in the σ direction, through the sides of the T-S grid cell. From (2.44c)

$$G_{\sigma,K} = 0 \quad , \quad (3.6e)$$

so that (3.6a) will be used to determine G_σ from G_λ and G_ϕ for all k . The quantity ω will never be needed.

The true vertical velocity w will not appear explicitly in the finite-difference equations. If w is desired it will be calculated from G_σ at points (i, j, k) using

$$\omega\alpha_z = G_\sigma + \overline{ua\delta\bar{\phi}\delta_i\bar{z}^{ik}} + \overline{va\bar{c}\delta\bar{\lambda}\delta_j\bar{z}^{jk}} \quad (3.7)$$

which is a finite-difference representation of the definition of ω (2.22a).

3.2.2 Heat and Salt Equations

The finite-difference approximations to the heat and salt equations (2.23b) and (2.23c) at points $i, j, k+\frac{1}{2}$ (see Figure 2) are

$$\begin{aligned} v\dot{T} = & \alpha_z \overline{\overline{z^{ij} \delta_k T^k}} - \delta_i (\overline{T^i} G_\lambda + Q_\lambda) - \delta_j (\overline{T^j} G_\phi + Q_\phi) \\ & - \delta_k (\overline{T^k} G_\sigma + Q_\sigma) + V\varepsilon \end{aligned} \quad (3.8)$$

and

$$\begin{aligned} v\dot{S} = & \alpha_z \overline{\overline{z^{ij} \delta_k S^k}} - \delta_i (\overline{S^i} G_\lambda + \Gamma_\lambda) - \delta_j (\overline{S^j} G_\phi + \Gamma_\phi) \\ & - \delta_k (\overline{S^k} G_\sigma + \Gamma_\sigma) \end{aligned} \quad (3.9)$$

The resolved volume fluxes G_λ , G_ϕ and G_σ have been defined in the previous section, and ε is a suitable numerical approximation to the distributed heat source. The quantities Q_λ , Q_ϕ , Q_σ , Γ_λ , Γ_ϕ and Γ_σ are the finite-difference representations of the sub-grid scale heat and salt fluxes at the cell sides. They are given by

$$Q_\lambda = q_\lambda \overline{\alpha_\lambda^j} \quad ,$$

$$Q_\phi = q_\phi \overline{\alpha_\phi^i} \quad ,$$

and

$$Q_\sigma = q_\sigma \alpha_z \quad , \quad (3.10a-c)$$

with similar expressions for Γ_λ , Γ_ϕ and Γ_σ in terms of γ_λ , γ_ϕ and γ_σ . The fluxes per unit area q_λ , q_ϕ and q_σ are defined at the appropriate cell sides by the finite-difference representation of q_λ , q_ϕ and q_z (2.25), and they are

$$q_\lambda = - \frac{\beta_H \bar{K}_H^i}{ac} \left(\frac{\delta_i T}{\delta \bar{\lambda}} - \frac{\delta_k \bar{T}^{ik}}{\delta_k \bar{z}^j} \frac{\delta_i \bar{z}^{ijk}}{\delta \bar{\lambda}} \right) ,$$

$$q_\phi = - \frac{\beta_H \bar{K}_H^j}{a} \left(\frac{\delta_j T}{\delta \bar{\phi}} - \frac{\delta_k \bar{T}^{jk}}{\delta_k \bar{z}^i} \frac{\delta_j \bar{z}^{ijk}}{\delta \bar{\phi}} \right) ,$$

$$q_z = - \beta_V \bar{K}_V^{ij} \frac{\delta_k T}{\delta_k \bar{z}^{ijk}} ,$$

and

$$q_\sigma = q_z - \frac{\bar{q}_\lambda^{ik}}{ac} \frac{\delta_i \bar{z}^j}{\delta \bar{\lambda}} - \frac{\bar{q}_\phi^{jk}}{a} \frac{\delta_j \bar{z}^i}{\delta \bar{\phi}} . \quad (3.11a-d)$$

The finite-difference representation of γ_λ , γ_ϕ , γ_z and γ_σ is identical with (3.11) but with T replaced by S . The locations at which q_λ and q_ϕ are defined are depicted in Figure 4.

The areas $\bar{\alpha}_\lambda^j$ and $\bar{\alpha}_\phi^i$, which multiply the sub-grid fluxes q_λ , q_ϕ , γ_λ and γ_ϕ in the definitions of Q_λ , Q_ϕ , Γ_λ and Γ_ϕ , represent the areas of the vertical T-S cell sides normal to the λ and ϕ directions. The contributions $\bar{q}_\lambda^{ik} a \delta \phi \delta_i \bar{z}^j$ and $\bar{q}_\phi^{jk} ac \delta \lambda \delta_j \bar{z}^i$ to the sub-grid heat flux Q_σ (and similar contributions to the salt flux Γ_σ) through the $\sigma = \text{constant}$ cell surfaces arise from the fact that fluxes in the λ and ϕ direction (at constant z) cross those surfaces.

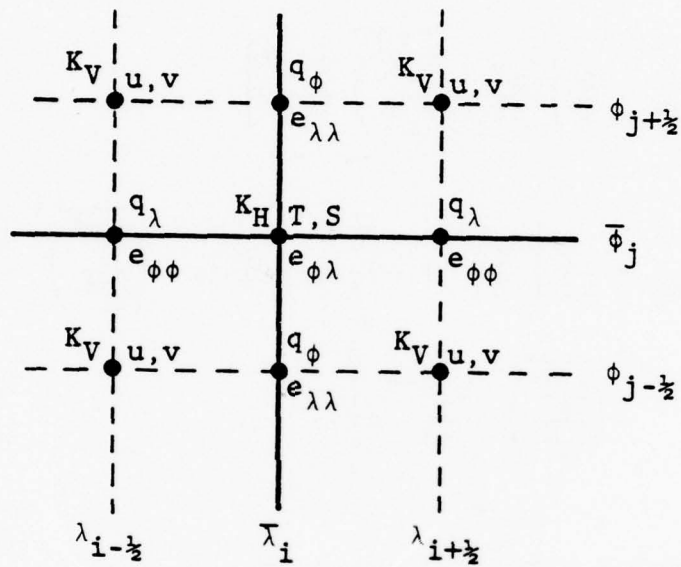


Figure 4. Arrangement of finite-difference sub-grid heat (and salt) fluxes, rate of strain components, and horizontal and vertical diffusivities in constant σ plane. The vertical diffusivity is displaced vertically.

The horizontal diffusivity K_H is computed from a representation of relevant components of the rate-of-strain tensor and (2.16). We approximate (see Figure 4)

$$e_{\lambda\lambda} = \frac{2}{ac} \left[\frac{\delta_i u}{\delta \lambda} - \left(\frac{\delta_k \bar{u}^k}{\delta_k z} \right)^i \frac{\delta_i \bar{z}^k}{\delta \lambda} - \bar{v}^i \right] , \quad (3.12a)$$

$$e_{\phi\phi} = \frac{2}{a} \left[\frac{\delta_i v}{\delta \phi} - \left(\frac{\delta_k \bar{v}^k}{\delta_k z} \right)^j \frac{\delta_j \bar{z}^k}{\delta \phi} \right] , \quad (3.12b)$$

and

$$e_{\phi\lambda} = \frac{1}{ac} \left[\frac{\delta_i \bar{v}^j}{\delta \lambda} + \frac{\delta_j \bar{u}^i}{\delta \phi} c + \bar{u}^{ij} s - \left(\frac{\delta_k \bar{v}^k}{\delta_k z} \right)^{ij} \frac{\delta_i \bar{z}^{jk}}{\delta \lambda} - \left(\frac{\delta_k \bar{u}^k}{\delta_k z} \right)^{ij} \frac{\delta_j \bar{z}^{ik}}{\delta \phi} c \right] . \quad (3.12c)$$

Then we define K_H at $(i, j, k+\frac{1}{2})$ as

$$K_H = \sqrt{2} (c_g \Delta)^2 \left[(e_{\lambda\lambda}^j)^2 + (e_{\phi\phi}^i)^2 + 2e_{\phi\lambda}^2 \right]^{\frac{1}{2}} . \quad (3.13)$$

We compute the vertical diffusivity K_V at points $(i+\frac{1}{2}, j+\frac{1}{2}, k)$, from a difference representation of (2.27) with N as given by (2.32a). We have

$$K_V = \ell^2(z) \left[\left(\frac{\delta_k u}{\delta_k z} \right)^2 + \left(\frac{\delta_k v}{\delta_k z} \right)^2 \right]^{\frac{1}{2}} (1-R/R_c)^{3/2} + C_V \exp(-z/z_V) ,$$

where

$$R = N^2 \left[\left(\frac{\delta_k u}{\delta_k \bar{z}^k} \right)^2 + \left(\frac{\delta_k v}{\delta_k \bar{z}^k} \right)^2 \right]^{-1}$$

$$R_c = 0.23$$

and

$$N^2 = \frac{g}{\rho_0} \left[\frac{\delta_k \bar{\rho}^{ij}}{\delta_k \bar{z}^k} - \bar{\rho}^{ijk} g \left(\frac{\partial \rho}{\partial p} \right)_{TS}^{ijk} \right] \quad (3.14a-d)$$

The quantity $(\partial \rho / \partial p)_{TS}$ is given by a representation of (2.32) described later. As mentioned earlier, we add a small, exponentially decreasing vertical diffusivity to account for those deep ocean regions where K_V as computed from (3.14) is very small or zero.

3.2.3 Horizontal Momentum Equations and the Hydrostatic Relation

The finite-difference approximations to the horizontal momentum equations (2.23d) and (2.23e) with the modified pressure terms (2.36) are (see Figure 4)

$$\begin{aligned} \bar{v}^{ij} \dot{u}^k &= \frac{\bar{\alpha}^{ij}}{\alpha_z \bar{z}^{ij}} \delta_k u^k - \frac{1}{2} \left[\delta_i (\bar{u}^i F_\lambda) + \bar{F}_\lambda \delta_i \bar{u}^i \right. \\ &+ \delta_j (\bar{u}^j F_\phi) + \bar{F}_\phi \delta_j \bar{u}^j + \delta_k (\bar{u}^k F_\sigma) + \bar{F}_\sigma \delta_k \bar{u}^k \left. \right] \\ &+ \delta_i (\tau_{\lambda\lambda} \bar{\alpha}_\lambda^i) + \delta_j (\tau_{\phi\lambda} \bar{\alpha}_\phi^j) + \delta_k (\tau_{\sigma\lambda} \bar{\alpha}_\sigma^k) \end{aligned}$$

(cont'd.)

$$\begin{aligned}
& + \bar{s} \bar{v}^{ij} \left[(uv - \overline{\tau_{\phi\lambda}^{ij}}) (\overline{ac})^{-1} \right] + fv\bar{v}^{ij} \\
& - (\alpha_{\lambda} \delta_i \bar{\pi}^{jk} - a\delta\bar{\phi}\delta_i \bar{z}^{ik} \delta_k \bar{\pi}^{ijkk}) \quad , \quad (3.15)
\end{aligned}$$

and

$$\begin{aligned}
\bar{v}^{ij\dot{v}} &= \overline{\alpha_z \bar{z}^{ij} \delta_k v}^k - \frac{1}{2} \left[\delta_i (\bar{v}^i F_{\lambda}) + \overline{F_{\lambda} \delta_i v}^i \right. \\
& + \delta_j (\bar{v}^j F_{\phi}) + \overline{F_{\phi} \delta_j v}^j + \delta_k (\bar{v}^k F_{\sigma}) + \overline{F_{\sigma} \delta_k v}^k \left. \right] \\
& + \delta_i (\overline{\tau_{\phi\lambda}^j \alpha_{\lambda}^i}) + \delta_j (\overline{\tau_{\phi\phi} \alpha_{\phi}^j}) + \delta_k (\overline{\tau_{\sigma\phi} \alpha_z^i j}) \\
& - \bar{s} \bar{v}^{ij} \left[(uu - \overline{\tau_{\lambda\lambda}^i}) (\overline{ac})^{-1} \right] - fu\bar{v}^{ij} \\
& - (\alpha_{\phi} \delta_j \bar{\pi}^{ik} - a\bar{c}\delta\bar{\lambda}\delta_j \bar{z}^{jk} \delta_k \bar{\pi}^{ijkk}) \quad . \quad (3.16)
\end{aligned}$$

The quantities F_{λ} , F_{ϕ} and F_{σ} are the resolved scale volume fluxes in the λ , ϕ and σ directions at the u-v cell sides. They are defined as

$$F_{\lambda} = \overline{u\alpha_{\lambda}^i} \quad ,$$

$$F_{\phi} = \overline{v\alpha_{\phi}^j} \quad ,$$

and

$$F_{\sigma} = \overline{G_{\sigma}^{ij}} \quad . \quad (3.17a-c)$$

The flux F_σ is computed as the i-j average of the σ fluxes of the four surrounding T-S cells in order to satisfy an energy conservation constraint which will be derived in a following section, and to avoid excessive F_σ values at the surface. With this definition of F_σ , the fluxes do not exactly satisfy a continuity relationship, that is,

$$\delta_i F_\lambda + \delta_j F_\phi + \delta_k F_\sigma \sim O(\Delta^2) \neq 0$$

where Δ is some measure of the grid spacing. However, the Piacsek and Williams (1970) approximation of the advection terms,

$$\frac{\partial}{\partial \lambda}(uF_\lambda) = \frac{1}{2} \left[\delta_i (\bar{u}^i F_\lambda) + \overline{F_\lambda \delta_i u^i} \right] / \delta \bar{\lambda} \quad , \quad (3.18)$$

ensures that a numerical representation of the total horizontal kinetic energy is conserved under advection.

The volume \bar{V}^{ij} ascribed to the u-v cell is the i-j average of the four adjacent T-S cells. This second-order approximation is necessary in order that numerical representations of the volume integrals of T , S , T^2 , S^2 and $(u^2 + v^2)/2$ may all be conserved under advection with z a function of time. This volume approximation also ensures that the sum of all T-S cell volumes is exactly equal to the sum of all u-v cell volumes. Note also that the area of the u-v cell normal to the vertical is the i-j average of the four adjacent T-S cells.

The horizontal sub-grid scale stresses $\tau_{\lambda\lambda}$, $\tau_{\phi\phi}$ and $\tau_{\phi\lambda}$ are computed at the same locations as $e_{\lambda\lambda}$, $e_{\phi\phi}$ and $e_{\phi\lambda}$, as described in Section 3.2.2 (see Figure 4).

Thus $\tau_{\lambda\lambda}$ and $\tau_{\phi\phi}$ represent average normal stresses over the vertical u-v cell faces normal to λ and ϕ . The shear stress $\tau_{\phi\lambda}$ is computed at the corners of the u-v cell (at the $k+\frac{1}{2}$ level), and it is appropriately averaged to yield the shear stresses on the vertical faces. The z- λ and z- ϕ stress components are computed at $i+\frac{1}{2}$, $j+\frac{1}{2}$, k, directly above the u-v points.

From (3.12) and (3.13) we have

$$\tau_{\lambda\lambda} = \overline{K_H^j} e_{\lambda\lambda} \quad ,$$

$$\tau_{\phi\phi} = \overline{K_H^i} e_{\phi\phi} \quad ,$$

and

$$\tau_{\phi\lambda} = K_H e_{\phi\lambda} \quad .$$

We also approximate, using (2.15) and (3.14),

$$\tau_{z\lambda} = K_V \frac{\delta_k u}{\delta_k \bar{z}^k} \quad ,$$

and

$$\tau_{z\phi} = K_V \frac{\delta_k v}{\delta_k \bar{z}^k} \quad . \quad (3.19a-e)$$

Then from (2.22d) and (2.22e)

$$\tau_{\sigma\lambda} = \tau_{z\lambda} - \frac{\overline{\tau_{\lambda\lambda}}^{ik}}{a\bar{c}} \frac{\delta_i \bar{z}^i}{\delta \bar{\lambda}} - \frac{\overline{\tau_{\phi\lambda}}^{ijk}}{a} \frac{\delta_j \bar{z}^j}{\delta \phi} \quad , \quad (3.19f)$$

and

$$\tau_{\sigma\phi} = \tau_{z\phi} - \frac{\overline{\tau_{\phi\lambda}}}{a\bar{c}} \frac{\overline{\delta_i z^i}}{\delta\bar{\lambda}} - \frac{\overline{\tau_{\phi\phi}}}{a} \frac{\delta_j \bar{z}^j}{\delta\bar{\phi}} \quad (3.19g)$$

The double-k averaging of Π in the numerical representation of $\partial\Pi/\partial\sigma$ in (3.15) and (3.16) is necessary to ensure that Conservation Property 4 is satisfied. We compute the Π gradients from a difference approximation to the hydrostatic relation (2.37) as follows.

We approximate the hydrostatic relation (2.37) at T-S grid points by

$$\delta_k \Pi = g \frac{\rho - \rho_r}{\rho_o} \delta_k \bar{z}^{ij} \quad (3.20a)$$

where the density ρ is given by the numerical implementation of the state equation as described in the next section, and

$$\rho_r = \rho_r(\bar{z}^{ijk}) \quad (3.20b)$$

Then formally

$$\Pi_k = g \sum_{m=2}^{k-1} \frac{\rho - \rho_r}{\rho_o} \delta_k \bar{z}^{ij} \Big|_{m+\frac{1}{2}} + \Pi_s \quad (3.21a)$$

where

$$\Pi_s = [p_a - p_r(\bar{z}_s^{ij})] / \rho_o \quad (3.21b)$$

To minimize rounding-error, however, we do not compute Π or $\bar{\Pi}^k$ directly. Instead, we obtain $\delta_i \bar{\Pi}^{jk}$ and $\delta_j \bar{\Pi}^{ik}$ at $k+\frac{1}{2}$ by applying the differencing and averaging operators to (3.21) to obtain, at $k+\frac{1}{2}$

$$\delta_i \bar{\Pi}^{jk} = g \overline{\sum_{m=2}^{k-1} \delta_i \left(\frac{\rho - \rho_r}{\rho_o} \delta_k \bar{z}^{ij} \right)^k} + \delta_i \Pi_s \quad (3.22a)$$

and

$$\delta_j \bar{\Pi}^{ik} = g \overline{\sum_{m=2}^{k-1} \delta_j \left(\frac{\rho - \rho_r}{\rho_o} \delta_j \bar{z}^{ij} \right)^k} + \delta_j \Pi_s \quad (3.22b)$$

so that the vertical summation is performed on the δ_i and δ_j differenced contributions to $\delta_i \Pi$ and $\delta_j \Pi$.

To compute $\delta_k \bar{\Pi}^{kk}$, we first compute $\delta_k \Pi$ at $k = 2\frac{1}{2}, 3\frac{1}{2}, \dots, K-\frac{1}{2}$ from (3.20). We introduce an additional grid level at $k=1$, above the ocean surface, and another at $k = K+1$, below the bottom; we compute Π at these levels by linear extrapolation. This is equivalent to the assumption that $\delta_k^2 \Pi = 0$ at $k=2$ and K . With these artificial Π values,

we compute $\delta_k \Pi$ at $k=1\frac{1}{2}$ and $K+\frac{1}{2}$. We then compute $\delta_k \bar{\Pi}^k$ at $k=2, 3, \dots, K$, and finally $\delta_k \bar{\Pi}^{kk}$ at $k=2\frac{1}{2}, 3\frac{1}{2}, \dots, K-\frac{1}{2}$. These values are averaged in i and j to yield $\delta_k \bar{\Pi}^{ijkk}$.

3.2.4 The Equation of State

We compute the density ρ from the equation of state (2.28) at T-S grid points. We obtain the pressure at those points from the difference equivalent of (2.35b) so that

$$\bar{p}^k = \rho_0 \bar{\pi}^k + \overline{p_r(z^{ij})}^k \quad . \quad (3.23)$$

Then P in (2.28a) is just

$$P = \bar{p}^k - 1.013 \text{ (bars)} \quad , \quad (3.24)$$

and ρ_t , K^0 , A and B are given directly by (2.31).

Similarly the quantity

$$\left(\frac{\partial \rho}{\partial P} \right)_{TS}$$

at T-S grid points is given directly by (2.32) with (3.23) and (3.24).

3.3 THE BOUNDARY CONDITIONS

In this section we describe the numerical implementation of the boundary conditions described in Section 2.5. The order of presentation parallels the discussion in that section. We describe the ocean surface and bottom conditions, and no-flux, flux and periodic lateral conditions.

We begin our discussion with the introduction of mesh lines just outside the forecast region.

3.3.1 Exterior Mesh Lines

The application of boundary conditions in our numerical scheme is facilitated through the use, in the usual manner, of mesh lines located outside the forecast region.

We introduced in the previous section σ mesh lines at $k=1$ and $K+1$ and $\bar{\sigma}$ mesh lines at $k=1\frac{1}{2}$ and $K+\frac{1}{2}$. To define z at the additional σ mesh levels, we require

$$z_1 = 2z_2 - z_3 \quad (3.25a)$$

and

$$z_{K+1} = 2z_K - z_{K-1} \quad (3.25b)$$

where the subscripts refer to k . With this definition, the local thickness of the additional exterior mesh "layers" is equal to the local thickness of the adjacent interior "layers".

We will also make use of exterior longitudinal and latitudinal mesh lines. We have already introduced the grid lines $\lambda_{1\frac{1}{2}}$, $\lambda_{I+\frac{1}{2}}$, $\phi_{1\frac{1}{2}}$ and $\phi_{J+\frac{1}{2}}$ which lie just outside the lateral boundaries of the forecast region. We define additional mesh lines

$$\bar{\lambda}_1 = 2\bar{\lambda}_2 - \bar{\lambda}_3 \quad ,$$

$$\bar{\lambda}_{I+1} = 2\bar{\lambda}_I - \bar{\lambda}_{I-1} \quad ,$$

$$\bar{\phi}_1 = 2\bar{\phi}_2 - \bar{\phi}_3 \quad ,$$

and

$$\bar{\phi}_{J+1} = 2\bar{\phi}_J - \bar{\phi}_{J-1} \quad . \quad (3.25c-f)$$

The exterior u-v grid cells (centered at $\lambda_{1\frac{1}{2}}$, $\lambda_{I+\frac{1}{2}}$, $\phi_{1\frac{1}{2}}$ and $\phi_{J+\frac{1}{2}}$) are thus equal in width, in terms of λ and ϕ , to the adjacent interior u-v cells.

The arrangement of the dependent variables T, S, u, v and z on the exterior mesh lines is identical to their arrangement in the interior which was described in Section 3.1.2. Values of these exterior quantities or expressions for them in terms of interior quantities, will be defined as required.

3.3.2 Ocean Surface Boundary Conditions

Analytic expressions for the ocean surface conditions were given in Section 2.5.1. We recall that the surface coincides with the σ mesh line at $k=2$, and, as before, we will denote quantities evaluated there with the subscript "s".

We represent the free-surface condition (2.39) by

$$\alpha \frac{\bar{z}}{z} \bar{z}_s^{ij} = G_{\sigma, k=2} - \alpha \frac{F}{z} F_s \quad (3.26)$$

for $i=2$ to I and $j=2$ to J , where $G_{\sigma, k=2}$ is obtained from the continuity equation (3.6). If \bar{z}_s is specified on any pair of λ and ϕ mesh lines, or if linear relations are defined along any pair of $\bar{\lambda}$ and $\bar{\phi}$ mesh lines between the values of \bar{z}_s on the neighboring λ and ϕ mesh lines, then \bar{z}_s is completely determined for all mesh locations $i+\frac{1}{2}$, $j+\frac{1}{2}$ from (3.26). We, therefore, might envision specifying, depending on the circumstance, \bar{z}_s along a pair of λ and ϕ exterior mesh lines or perhaps specifying $\delta_i \bar{z}_s$ and $\delta_j \bar{z}_s$ along a pair of $\bar{\lambda}$ and $\bar{\phi}$ boundary mesh lines, then computing \bar{z}_s . We would, however, encounter serious difficulties with this procedure - rounding error would rapidly accumulate during the computation and render the calculated \bar{z}_s values meaningless.

To alleviate the rounding error problem, we will obtain \bar{z}_s from

$$\bar{z}_s^{ij} = \frac{G_{\sigma, k=2} - F_s^{ij}}{\alpha \frac{z}{z}} \quad (3.27)$$

which is the i-j average of (3.26). Equation (3.27) is defined at the interior mesh points $i = 2\frac{1}{2}, 3\frac{1}{2}, \dots, I-\frac{1}{2}$ and $j = 2\frac{1}{2}, 3\frac{1}{2}, \dots, J-\frac{1}{2}$. To determine \dot{z}_S from (3.27) we must specify appropriate conditions on \dot{z}_S at all lateral boundaries. Such conditions include the specification of $\delta_i \dot{z}_S$ and $\delta_j \dot{z}_S$ or \bar{z}_S^i and \bar{z}_S^j at $\bar{\lambda}$ and $\bar{\phi}$ boundary mesh lines. The former conditions will be used at no-flux boundaries and the latter at flux boundaries. Periodic conditions in longitude are also appropriate. With suitable boundary conditions (3.27) is easily solved in two successive tridiagonal inversions.

We must point out here that \dot{z}_S as computed from (3.27) will not exactly satisfy (3.26) since the i-j averaging of $G_{\sigma, k=2}/\alpha_z - F_S$ filters it of components which vary as $(-1)^i$ and $(-1)^j$. The difference, however, is very slight and will henceforth be ignored.

The numerical representation of the surface temperature conditions (2.40) and (2.41) is facilitated by the use of artificial T values at $k=1\frac{1}{2}$. We represent (2.40) simply by

$$\bar{T}_{k=2}^k = T_S \quad (3.28)$$

where T_S is a specified surface temperature distribution. The heat flux condition (2.41) is simply

$$q_{k=2} = q_S \quad (3.29)$$

The numerical representation of the surface salinity condition (2.42) is similar to (3.29). We approximate (2.42)

$$\gamma_{k=2} = - \sum_{k=2}^k F_s \quad (3.30)$$

where F_s is the water flux into the ocean.

We approximate the surface wind stress conditions (2.43a) and (2.43b) by

$$\tau_{\sigma\lambda, k=2} = - C_D u_a \frac{\rho_a}{\rho_o} \left(u_a^2 + v_a^2 \right)^{\frac{1}{2}}, \quad (3.31a)$$

and

$$\tau_{\sigma\phi, k=2} = - C_D v_a \frac{\rho_a}{\rho_o} \left(u_a^2 + v_a^2 \right)^{\frac{1}{2}}, \quad (3.31b)$$

where u_a and v_a are numerical representations of the local surface wind components.

Finally, the numerical counterpart to the surface pressure condition (2.43c) is simply

$$\Pi_s = \left[p_a - p_r(\overline{z_s^{ij}}) \right] / \rho_o \quad (3.31c)$$

at points (i,j) , where p_a is specified.

3.3.3 Ocean Bottom Boundary Conditions

Analytic expressions for the ocean bottom conditions were given in Section 2.5.2. We recall that the bottom coincides with the σ mesh line at $k=K$.

We represent the bottom kinematic condition (2.44) by simply

$$G_{\sigma, k=K} = 0 \quad (3.32)$$

The bottom conditions on T and S given in (2.45) and (2.46) are approximated with the aid of artificial values at $K+\frac{1}{2}$ by

$$q_{\sigma} = 0 \quad (3.33a)$$

and

$$\gamma_{\sigma} = 0 \quad (3.33b)$$

at $k=K$, where q_{σ} is given by (3.11d) and γ_{σ} by the γ -counterpart to (3.11d). The terms in (3.11d) which were eliminated at the surface as described in the previous section to yield the simplified expressions, (3.29) and (3.30), for the surface conditions may not in general be eliminated at the bottom.

Finally, we approximate the bottom conditions on u and v, (2.47), at $k=K$, with the aid of artificial values of u and v at $K+\frac{1}{2}$, by

$$\bar{u}^k + \delta_k z \delta_k u/d = 0 \quad ,$$

and

$$\bar{v}^k + \delta_k z \delta_k v/d = 0 \quad ,$$

where

$$d = \left[\frac{u^2 + v^2}{N^2 + f^2} \right]^{\frac{1}{2}} \quad , \quad (3.34a-c)$$

is evaluated at $K-\frac{1}{2}$ with N^2 as given by (3.14d) at $K-1$. For the sake of numerical convenience, we have chosen to evaluate elements of (3.34) at slightly different locations. The characteristics of these conditions, which were described in Section 2.5.2, are unaffected.

3.3.4 No-Flux Lateral Boundary Conditions

Analytic expressions for the no-flux lateral boundary conditions were presented in Section 2.5.3. Their finite-difference representation is greatly simplified with the application of the conditions

$$\delta_i z = 0 \quad \text{along longitudinal boundaries} \quad (3.35a)$$

and

$$\delta_j z = 0 \quad \text{along latitudinal boundaries} \quad , \quad (3.35b)$$

for all k . Conditions (3.35) will be satisfied for all k if they are satisfied at the surface $k=2$ and at the bottom (assuming that the transformation parameter δ is a constant). We assume that they are satisfied at the bottom; then we need only apply (3.35) to the calculation of the surface elevation from (3.27).

The finite-difference counterparts to the longitudinal boundary conditions (2.48) are

$$\delta_i \bar{T}^i = 0 \quad ,$$

$$\delta_i \bar{S}^i = 0 \quad ,$$

$$\bar{u}^i = 0 \quad ,$$

and

$$\delta_i v = 0 \quad . \quad (3.36a-d)$$

The conditions on T and S are obtained from (3.11a) with the application of (3.35a).

The finite-difference counterparts to the latitudinal conditions (2.49) are

$$\delta_j \bar{T}^j = 0 \quad ,$$

$$\delta_j \bar{S}^j = 0 \quad ,$$

$$\bar{v}^j = 0 \quad ,$$

and

$$\delta_j u = 0 \quad . \quad (3.37a-d)$$

The conditions on T and S are obtained from (3.11b) with the aid of (3.35b).

3.3.5 Flux Lateral Boundary Conditions

We represent the inflow conditions (2.50) at a longitudinal boundary by

$$T, S, \bar{u}^i, \bar{v}^i \text{ and } \bar{z}_S^i \text{ specified ;} \quad (3.38a-e)$$

and at a latitudinal boundary by

$$T, S, \bar{u}^j, \bar{v}^j \text{ and } \bar{z}_S^j \text{ specified .} \quad (3.39a-e)$$

We represent the longitudinal boundary outflow conditions (2.51) by

$$\delta_i^2 T = 0 \quad ,$$

$$\delta_i^2 S = 0 \quad ,$$

$$\delta_i^2 v = 0 \quad ,$$

and

$$\bar{u}^i \text{ and } \bar{z}_S^i \text{ specified ;} \quad (3.40a-e)$$

and we represent the latitudinal conditions (2.52) by

$$\delta_j^2 T = 0 \quad ,$$

$$\delta_j^2 S = 0 \quad ,$$

$$\delta_j^2 u = 0 \quad ,$$

and

$$\bar{v}^j \text{ and } \bar{z}_S^j \text{ specified .} \quad (3.41a-e)$$

We note that the outflow conditions $\delta_i^2 v = 0$ and $\delta_j^2 u = 0$ are applied, not at the boundary, but at the u-v point just inside the boundary.

3.3.6 Periodicity Conditions in Longitude

To represent the longitudinal periodicity conditions (2.53) we set

$$\lambda_{1\frac{1}{2}} = \lambda_{I-\frac{1}{2}} - 2\pi \quad (3.42a)$$

and

$$\lambda_{I+\frac{1}{2}} = \lambda_{2\frac{1}{2}} + 2\pi \quad (3.42b)$$

with the requirements that

$$\bar{\lambda}_2 = 0$$

and

$$\bar{\lambda}_I = 2\pi$$

Then we require

$$\left. \begin{aligned} z_{1\frac{1}{2}} &= z_{I-\frac{1}{2}} \\ z_{I+\frac{1}{2}} &= z_{2\frac{1}{2}} \end{aligned} \right\} ,$$

$$\left. \begin{aligned} T_1 &= T_{I-1} \\ T_I &= T_2 \end{aligned} \right\} ,$$

$$\left. \begin{aligned} s_1 &= s_{I-1} \\ s_I &= s_2 \end{aligned} \right\} ,$$

$$\left. \begin{aligned} u_{1\frac{1}{2}} &= u_{I-\frac{1}{2}} \\ u_{I+\frac{1}{2}} &= u_{2\frac{1}{2}} \end{aligned} \right\} ,$$

and

$$\left. \begin{aligned} v_{1\frac{1}{2}} &= v_{I-\frac{1}{2}} \\ v_{I+\frac{1}{2}} &= v_{2\frac{1}{2}} \end{aligned} \right\} , \tag{3.42c-g}$$

for all j and k. The subscripts in (3.42) refer to i. Equation (3.42c) is applied as a boundary condition on z_s in the solution of (3.27).

Section 4

DIFFERENCE-SCHEME CONSERVATION PROPERTIES

In this section we demonstrate that our finite-difference scheme has the four conservation properties described in Section 3. Since the equations of heat and salt conservation are formally identical, except for the source term which is neglected in the analysis presented in this section, the salt equation will not be considered explicitly.

4.1 SUMMATION DEFINITIONS AND RELATIONS

The derivation of the conservation properties is facilitated by the following summation definitions. Let f be a function defined at the integer points $i = 1, 2, \dots, I, I+1$, and let g be defined at the "half-integer" points $i = 1\frac{1}{2}, 2\frac{1}{2}, \dots, I-\frac{1}{2}, I+\frac{1}{2}$, and let the boundaries of a region be at $i = 2$ and I . We then define three summation operations, as follows:

$$\sum_i f \equiv f_2 + f_3 + \dots + f_I, \quad (4.1)$$

that is, the sum over all values of f in the interior and on the boundaries of the region;

$$\sum'_i f \equiv \frac{1}{2}f_2 + f_3 + \dots + f_{I-1} + \frac{1}{2}f_I, \quad (4.2)$$

that is, the sum over all f with the boundary contributions f_2 and f_I halved; and

$$\sum_i^h g \equiv g_{2\frac{1}{2}} + g_{3\frac{1}{2}} + \dots + g_{I-\frac{1}{2}}, \quad (4.3)$$

that is, the sum over all interior values of g . The sums $\sum_i f$ and $\sum_i^h g$ are analogs of the respective integrals.

We present summation relations based on these three definitions below. A property of our two-point averaging and differencing operators, which we make use of in the derivation of the relations, is

$$\bar{h}^i \delta_i h = \frac{1}{2} \delta_i h^2, \quad (4.4)$$

where h is either f or g . Property (4.4) is easily derived. We also make use of the Piacsek and Williams notation

$$\widetilde{hh}^i = h_{i+\frac{1}{2}} h_{i-\frac{1}{2}},$$

which approximates the square of h at grid point i .

The summation relations which we apply in the demonstration of the conservation properties of our difference scheme are presented in Table 4.1. In these relations

$$\left[f \right]_2^I \equiv f_I - f_2.$$

Relations (S.3) through (S.8) are all obtained from (4.4), (S.1) and (S.2); (S.1) and (S.2) are difference calculus counterparts to integration by parts, and they are easily derived.

TABLE 4.1 SUMMATION RELATIONS

One Dimension

$$\sum_i^{\prime} f \bar{g}^i - \sum_i^h g \bar{f}^i = \frac{1}{2} \left[f \delta_i g \right]_2^I \quad (\text{S.1})$$

$$\sum_i^{\prime} f \delta_i g + \sum_i^h g \delta_i f = \left[f \bar{g}^i \right]_2^I \quad (\text{S.2})$$

$$\sum_i^h (\overline{f \delta_i g}^i + g \delta_i f) = \left[f \bar{g}^i \right]_2^I \quad (\text{S.3})$$

$$\sum_i^{\prime} (f \delta_i (\bar{f}^i g) - \frac{1}{2} f^2 \delta_i g) = \frac{1}{2} \left[\overline{f f^i g}^i \right]_2^I \quad (\text{S.4})$$

$$\sum_i^h (g \delta_i (\bar{g}^i f) - \frac{1}{2} g^2 \delta_i f) = \frac{1}{2} \left[f \widetilde{g g}^i \right]_2^I \quad (\text{S.5})$$

$$\sum_i^h (\overline{g f \delta_i g}^i + \frac{1}{2} g^2 \delta_i f) = \frac{1}{2} \left[f \widetilde{g g}^i \right]_2^I \quad (\text{S.6})$$

$$\sum_i^h (g \delta_i (\bar{g}^i f) + \overline{g f \delta_i g}^i) = \left[f \widetilde{g g}^i \right]_2^I \quad (\text{S.7})$$

TABLE 4.1 Continued

$$\sum_i^h (g \delta_i \bar{f}^{ii} + \bar{f}^i \delta_i \bar{g}^i) = \left[\bar{g}^i \bar{f}^{ii} - \frac{1}{4} \delta_i \bar{f}^i \delta_i \bar{g} \right]_2^I \quad (\text{S.8})$$

Two Dimensions

$$\begin{aligned} \sum_i^h \sum_j^h \bar{f} \bar{g}^{ij} - \sum_i^h \sum_j^h g \bar{f}^{ij} \\ = \frac{1}{4} \sum_i^h \left[\bar{f}^i \delta_i \bar{g} \right]_2^J + \frac{1}{4} \sum_j^h \left[\bar{f}^j \delta_j \bar{g} \right]_2^I + \left[f \delta_i \delta_j \bar{g} / 16 \right]_{2,2}^{I,J} \end{aligned} \quad (\text{S.9})$$

$$\begin{aligned} \sum_i^h \sum_j^h f \delta_i \bar{g}^j + \sum_i^h \sum_j^h g \delta_i \bar{f}^j \\ = \sum_j^h \left[\bar{f}^j \bar{g}^i \right]_2^I - \frac{1}{4} \sum_i^h \left[\delta_i f \delta_j \bar{g} \right]_2^J + \frac{1}{4} \left[f \delta_j \bar{g}^i \right]_{2,2}^{I,J} \end{aligned} \quad (\text{S.10})$$

Note that in these relations

$$\left[f \right]_2^I = f_I - f_2 \quad ,$$

and

$$\widetilde{hh}^i = h_{i+\frac{1}{2}} h_{i-\frac{1}{2}}$$

where h is either f or g.

As an example of the manipulations required to derive (S.3) through (S.8), we present the derivation of (S.3). We rearrange (S.1) with g , as it appears in (S.1), replaced by unity and f replaced by $f\delta_i g$ as

$$\sum_i^h \overline{f\delta_i g^i} = \sum_i' f\delta_i g ,$$

since $\delta_i 1 = 0$, and we rearrange (S.2) as

$$\sum_i^h g\delta_i f = -\sum_i' f\delta_i g + [fg^{-i}]_2^I .$$

We add these two equations to obtain

$$\sum_i^h (\overline{f\delta_i g^i} + g\delta_i f) = [fg^{-i}]_2^I ,$$

relation (S.3).

With similar manipulations, we derive (S.4) and (S.5) from (S.2) with the aid of (4.4), (S.6) from (S.1) and (S.2) with the aid of (4.4), (S.7) from (S.5) and (S.6), and (S.8) from (S.1) and (S.2).

If we assume that f is defined also at the j integer points, $j = 1, 2, \dots, J, J+1$, and g at the j "half-integer" points $j = 1\frac{1}{2}, 2\frac{1}{2}, \dots, J-\frac{1}{2}, J+\frac{1}{2}$, we easily obtain (S.9) which is the two-dimensional counterpart of (S.1). We may also derive a two-dimensional "integration-by-parts" relation (S.10), from (S.1) and (S.2).

We first show that, in the absence of explicit source terms, the temporal rate of change of VT (and VS) as computed from the difference equation and summed over all (T-S) grid points is exactly equal to the net flux of T into the computational region.

We rewrite equation (3.8) with V taken within the time derivative, and with the source term ϵ neglected, as

$$\begin{aligned} \frac{\partial}{\partial t}(VT) &= \alpha_z \delta_k \bar{z}^{ij} T + \alpha_z \overline{\bar{z}^{ij} \delta_k T}^k \\ &\quad - \delta_i (\bar{T}^i G_\lambda + Q_\lambda) - \delta_j (\bar{T}^j G_\phi + Q_\phi) - \delta_k (\bar{T}^k G_\sigma + Q_\sigma) \dots * \quad (4.5) \end{aligned}$$

We sum (4.5) over all the grid points with the lateral boundary contributions to the sum halved since only half the volume of a boundary T-S cell is within the computational region. We apply (S.3) in k to the first two terms on the right-hand side involving \bar{z} (since α_z is independent of k), and we apply (S.2) in k to the last term on the right-hand side; we obtain

$$\begin{aligned} \sum_i \sum_j \sum_k^h \frac{\partial}{\partial t}(VT) &= \sum_i \sum_j \left\{ \left[\bar{T}^k (\alpha_z \bar{z}^{ij} - G_\sigma) - Q_\sigma \right]_2^K \right. \\ &\quad \left. - \sum_k^h \left[\delta_i (\bar{T}^i G_\lambda + Q_\lambda) + \delta_j (\bar{T}^j G_\phi + Q_\phi) \right] \right\} \dots \quad (4.6) \end{aligned}$$

*The notations $\partial f / \partial t$ and \dot{f} for the time derivative of $f(t)$ are used where convenient.

We next apply (S.2) in i and j to the i and j flux terms respectively; we make use of the conditions that \dot{z} , G_σ and q_σ are identically zero at the ocean bottom and that, from (3.26),

$$\alpha_z \bar{z}^{ij} = G_\sigma - \alpha_z F_S$$

at the surface. We obtain the difference counterpart to (2.54),

$$\begin{aligned} \sum_i \sum_j \sum_k^h \frac{\partial}{\partial t} (VT) = & \sum_i \sum_j \left[\alpha_z F_S \bar{T}^k + Q_\sigma \right]_{k=2} \\ & + \sum_k^h \left\{ \sum_j \left[\bar{T}^i G_\lambda^i + \bar{Q}_\lambda^i \right]_2^I + \sum_i \left[\bar{T}^j G_\phi^j + \bar{Q}_\phi^j \right]_2^J \right\} \end{aligned}$$

(4.7)

The terms summed over k on the right-hand side of (4.7) represent the fluxes of T , both resolved and sub-grid scale, through the lateral boundaries; the ij sum of $\left[\alpha_z F_S \bar{T}^k + Q_\sigma \right]_{k=2}$ represents the heat flux. Thus, the conservation property is established - the rate of change of VT summed over all grid points exactly equals the flux of T through the region boundaries.

With the application at $i = 2$ and I of either no-flux or periodic conditions as described in Sections 3.3.4 and 3.3.6 respectively, and the application at $j = 2$ and J of no-flux conditions, the net contribution to the sum of the horizontal fluxes vanishes. We obtain

$$\sum_i \sum_j \sum_k^h \frac{\partial}{\partial t} (vT) = \sum_i \sum_j (\alpha_{zF} \bar{T}^k + Q_{\sigma})_{k=2} , \quad (4.8)$$

so that the total rate of increase of the heat in the region is equal to the flux through the ocean surface. With a distributed heat source ϵ , its volume sum is added to the right-hand side of this equation.

4.3 CONSERVATION OF VT^2 AND VS^2 BY ADVECTION
(CONSERVATION PROPERTY 2)

Next we show that under the action of the advection terms the temporal rate of change of VT^2 summed over all T-S grid points is exactly zero.

We neglect the sub-grid fluxes in (4.5) so that that equation becomes simply a statement of the conservation of VT by resolved-scale advection. We multiply by T and sum over all grid points to obtain

$$\sum_i \sum_j \sum_k^h \frac{\partial}{\partial t} (\frac{1}{2} VT^2) = \sum_i \sum_j \sum_k^h \left\{ \frac{1}{2} T^2 \alpha_z \delta_k \bar{z}^{ij} + \alpha_z T \overline{\bar{z}^{ij} \delta_k T}^k - T \left[\delta_i (\bar{T}^i G_\lambda) + \delta_i (\bar{T}^j G_\phi) + \delta_k (\bar{T}^k G_\sigma) \right] \right\} . \quad (4.9)$$

We apply (S.6) in k to the second term on the right-hand side and in k to the last term, $-T \delta_k (\bar{T}^k G_\sigma)$. Then, with the aid of the surface and bottom conditions (3.26) and (3.32), we obtain

$$\sum_i \sum_j \sum_k^h \frac{\partial}{\partial t} (\frac{1}{2} VT^2) = \sum_i \sum_j \left\{ \frac{1}{2} \tilde{T}^k \alpha_z F_s^k - \sum_k^h \left[T \delta_i (\bar{T}^i G_\lambda) + T \delta_j (\bar{T}^j G_\phi) + \frac{1}{2} T^2 \delta_k G_\sigma \right] \right\} . \quad (4.10)$$

The first term on the right in (4.10) represents the flux of T^2 through the surface.

We next apply (S.5) to the horizontal flux terms in (4.10) so that

$$\begin{aligned} \sum_i \sum_j \sum_k^h \frac{\partial}{\partial t} (\frac{1}{2} v_T^2) &= - \sum_i \sum_j \sum_k^h \frac{1}{2} T^2 (\delta_i G_\lambda + \delta_j G_\phi + \delta_k G_\sigma) \\ &\quad - \sum_k^h \left\{ \sum_j \frac{1}{2} |\overline{T T^i G_\lambda}|_2^I + \sum_i \frac{1}{2} |\overline{T T^j G_\phi}|_2^J \right\} \\ &\quad + \sum_i \sum_j \frac{1}{2} \overline{T T^k}_{k=2} \alpha_z F_s \end{aligned} \quad (4.11)$$

The first group of terms on the right-hand side of (4.11) represents the net generation of v_T^2 by the advection terms; since

$$\delta_i G_\lambda + \delta_j G_\phi + \delta_k G_\sigma = 0$$

by continuity, there is zero net generation and the conservation property is established. Equation (4.11) is the difference counterpart to (2.55).

The remaining terms in (4.11) represent the flux of T^2 across the region boundaries; the lateral contributions vanish with the application of either the no-flux or

periodic conditions at the longitudinal boundaries and the no-flux condition at the latitudinal boundaries. Under these conditions, with sub-grid fluxes and heat sources neglected and with $F_s = 0$,

$$\sum_i \sum_j \sum_k^h \frac{\partial}{\partial t} (\frac{1}{2} v T^2) = 0 \quad . \quad (4.12)$$

4.4 CONSERVATION OF HORIZONTAL KINETIC ENERGY BY ADVECTION, AND CONVERSION OF KINETIC ENERGY TO POTENTIAL ENERGY (CONSERVATION PROPERTIES 3 AND 4)

In this final section we consider the finite-difference representation of the horizontal-flow kinetic energy, which is the sum over all u-v grid points of $\frac{1}{2}\bar{v}^{ij}(u^2+v^2)$. We first demonstrate that its time rate of change under the action of the advection terms is zero (Conservation Property 3). Secondly, we show that its rate of increase under the action of the horizontal pressure gradient is equal to a natural representation of the rate of working by the buoyancy forces (Conservation Property 4).

We neglect the sub-grid stress terms in (3.15) and (3.16), multiply (3.15) by u, (3.16) by v, rearrange the left-hand side so \bar{v}^{ij} is taken within the time derivative, add the two resulting equations together, and sum over all u-v grid points to obtain

$$\frac{\partial}{\partial t} \sum_i^h \sum_j^h \sum_k^h \frac{1}{2} \bar{v}^{ij} (u^2 + v^2) = I_1 + I_2 + I_3 \quad , \quad (4.13)$$

where

$$I_1 \equiv \sum_i^h \sum_j^h \sum_k^h \left\{ \frac{1}{2} (u^2 + v^2) \overline{\alpha_z \delta_k \bar{z}^{ij}}^{ij} + u \overline{\alpha_z \bar{z}^{ij}}^{ij} \delta_k^k u \right. \\ \left. + v \overline{\alpha_z \bar{z}^{ij}}^{ij} \delta_k^k v \right\}$$

$$\begin{aligned}
I_2 \equiv & -\frac{1}{2} \sum_i^h \sum_j^h \sum_k^h \left\{ u \delta_i (\bar{u}^i F_\lambda) + \overline{u F_\lambda \delta_i u^i} + v \delta_i (\bar{v}^i F_\lambda) + \overline{v F_\lambda \delta_i v^i} \right. \\
& + u \delta_j (\bar{u}^j F_\phi) + \overline{u F_\phi \delta_j u^j} + v \delta_j (\bar{v}^j F_\phi) + \overline{v F_\phi \delta_j v^j} \\
& \left. + u \delta_k (\bar{u}^k F_\sigma) + \overline{u F_\sigma \delta_k u^k} + v \delta_k (\bar{v}^k F_\sigma) + \overline{v F_\sigma \delta_k v^k} \right\} , \quad (4.15)
\end{aligned}$$

and

$$\begin{aligned}
I_3 \equiv & \sum_i^h \sum_j^h \sum_k^h \left\{ -u \alpha_\lambda \delta_i \bar{\Pi}^{jk} - v \alpha_\phi \delta_j \bar{\Pi}^{ik} \right. \\
& \left. + (u a \delta_\phi \delta_i \bar{z}^{ik} + v a \delta_\lambda \delta_j \bar{z}^{jk}) \delta_k \bar{\Pi}^{ijkk} \right\} . \quad (4.16)
\end{aligned}$$

We treat the I_1 , I_2 and I_3 sums in turn. Sums I_1 and I_2 together represent the generation of kinetic energy by the advection terms, and the net flux of energy across the region boundaries. Sum I_3 represents the work done by the pressure forces.

We first consider I_1 . We apply (S.6) in k to the second and third terms in I_1 (remember α_z is independent of k), and I_1 simplifies immediately to

$$I_1 = \frac{1}{2} \sum_i^h \sum_j^h \left[\alpha_z \bar{z}^{ij} \right]_2^{ij} (\bar{u}^k + \bar{v}^k) \quad (4.17)$$

Next, we consider I_2 . We apply (S.6) in i to the first four terms, in j to the second four terms, and in k to the last four terms to obtain

$$\begin{aligned}
 I_2 = & -\frac{1}{2} \sum_k^h \left\{ \sum_j^h \left[F_\lambda (\bar{u}u^i + \bar{v}v^i) \right]_2^I + \sum_i^h \left[F_\phi (\bar{u}u^j + \bar{v}v^j) \right]_2^J \right. \\
 & \left. - \frac{1}{2} \sum_i^h \sum_j^h \left[F_\sigma (\bar{u}u^k + \bar{v}v^k) \right]_2^K \right\} \quad (4.18)
 \end{aligned}$$

We recall that

$$F_\sigma = \bar{G}_\sigma^{-ij} ,$$

and we apply (3.26) and (3.32) to (4.17) and combine the resulting expression for I_1 with (4.18) to obtain

$$\begin{aligned}
 I_1 + I_2 = & \frac{1}{2} \sum_i^h \sum_j^h \left[\bar{\alpha}_z F_s^{-ij} (\bar{u}u^k + \bar{v}v^k) \right]_{k=2} \\
 & + \frac{1}{2} \sum_k^h \left\{ \sum_j^h \left[F_\lambda (\bar{u}u^i + \bar{v}v^i) \right]_I^2 + \sum_i^h \left[F_\phi (\bar{u}u^j + \bar{v}v^j) \right]_J^2 \right\} \quad (4.19)
 \end{aligned}$$

All of the terms in (4.19) represent energy fluxes at the boundaries of our region so that there is no internal generation of energy by the advection terms.

Thus Conservation Property 3 is demonstrated. We were able to obtain this result without the application of a continuity relation as a result of our use of the Piacsek-Williams advection operator (3.18). Thus we do not require

$$\delta_i F_\lambda + \delta_j F_\phi + \delta_k F_\sigma = 0 \quad ,$$

and this relation is only approximately true to second order in the mesh spacing.

The interpretation of the terms in (4.19) is straightforward and their differential counterparts may be found in (2.56). The first expression (that summed over both i and j) represents the flux of kinetic energy across the ocean surface. Our computation of F_σ as the i - j average of G_σ is partially motivated by the constraint that the kinetic energy flux across the surface be exactly zero when $F_s = 0$. The remaining terms in equation (4.19) clearly represent the flux of kinetic energy across the longitudinal and latitudinal boundaries.

With the application of either the no-flux or periodicity conditions at the longitudinal boundaries, and the no-flux conditions at the latitudinal boundaries, we obtain simply

$$I_1 + I_2 = \frac{1}{2} \sum_i^h \sum_j^h \frac{1}{\alpha_z F_s} {}^{ij} (\overline{uu^k} + \overline{vv^k})_{k=2} \quad .$$

Finally, we consider the pressure-work sum I_3 . We apply (S.10) and i and j to the first two terms in (4.16) and (S.9) in i and j to the last two to obtain

$$\begin{aligned}
I_3 = & \sum_i \sum_j I_4 \\
& + \sum_k^h \left\{ \sum_j^h \left[\frac{1}{2} \delta_j \bar{\pi}^k \delta_i (v \alpha_\phi) - \bar{\pi}^{jk} F_\lambda - \frac{1}{2} \delta_k \bar{\pi}^{jkk} \delta_i W \right]_2^I \right. \\
& + \sum_i^h \left[\frac{1}{2} \delta_i \bar{\pi}^k \delta_j (u \alpha_\lambda) - \bar{\pi}^{ik} F_\phi - \frac{1}{2} \delta_k \bar{\pi}^{ikk} \delta_j W \right]_2^J \\
& \left. - \left[\frac{1}{2} \bar{\pi}^k (\delta_j F_\lambda + \delta_i F_\phi) + \delta_k \bar{\pi}^{kk} \delta_i \delta_j W / 16 \right]_2^I \right. \left. \right]_2^J \quad (4.20)
\end{aligned}$$

where

$$I_4 = \sum_k^h \left\{ \bar{w}^{ij} \delta_k \bar{\pi}^{kk} + (\delta_i G_\lambda + \delta_j G_\phi) \bar{\pi}^k \right\} \quad (4.21)$$

and

$$W \equiv u a \delta \bar{\phi} \delta_i \bar{z}^{ik} + v a \bar{c} \delta \bar{\lambda} \delta_j \bar{z}^{jk} \quad (4.22)$$

The terms in (4.20) evaluated at the lateral boundaries represent the work done by the pressure on the lateral boundary fluxes. The remaining term, the i-j sum of I_4 , is the work done by the pressure forces in the interior and at the surface. From continuity (3.6)

$$I_4 = \sum_k^h \left\{ \bar{w}^{ij} \delta_k \bar{\pi}^{kk} - \delta_k G_\sigma \bar{\pi}^k \right\} \quad (4.23)$$

We apply (S.8) in k to the term involving \bar{w}^{ij} in (4.23) so that

$$I_4 = \sum_k^h \left\{ -\bar{\pi}^k (\delta_k \bar{w}^{ijk} + \delta_k G_\sigma) \right\} + \left[\bar{\pi}^{kk} \bar{w}^{ijk} - \frac{1}{2} \delta_k \bar{\pi}^k \delta_k \bar{w}^{ij} \right]_2^K \quad (4.24)$$

Then since from (3.7)

$$\alpha_z w = G_\sigma + \bar{w}^{ijk} \quad (4.25)$$

we apply (S.2) to obtain

$$I_4 = \sum_k \left\{ \alpha_z w \delta_k \bar{\pi}^k \right\} + \left[\bar{\pi}^{kk} (\bar{w}^{ijk} - \alpha_z w) - \frac{1}{2} \delta_k \bar{\pi}^k \delta_k \bar{w}^{ij} \right]_2^K \quad (4.26)$$

The first term in (4.26), $\alpha_z w \delta_k \bar{\pi}^k$, represents the work done by the buoyancy forces and the conversion of potential energy to horizontal kinetic energy, in analogy with the equivalent term in the integral expression (2.56). We simplify the second term by applying (4.25) and the surface and bottom conditions (3.26) and (3.32) so that

$$\left[\bar{\pi}^{kk} (\bar{w}^{ijk} - \alpha_z w) \right]_2^K = \alpha_z (\bar{z}_s^{ij} + F_s) \bar{\pi}_{k=2}^{kk} \quad (4.27)$$

which is the work done by the surface pressure at the moving surface (since with the linear extrapolation procedure described earlier, $\bar{\Pi}_{k=2}^{kk} = \Pi_s$).

The remaining term

$$\left[\frac{1}{2} \delta_k \bar{\Pi}_k \delta_k \bar{W}^{ij} \right]_2^K$$

is exactly zero under the boundary condition that $\delta_k \bar{W}^{ij} = 0$ at $k=2$ and K . The conditions imply that w is defined and computed from

$$w = (G_{\sigma, k=2} + \bar{W}_{K=2\frac{1}{2}}^{ij}) / \alpha_z \quad \text{at } k=2 \quad (4.28a)$$

and

$$w = (G_{\sigma, K} + \bar{W}_{K-\frac{1}{2}}^{ij}) / \alpha_z \quad \text{at } k=K \quad (4.28b)$$

We may now combine (4.26), (4.27) and the conditions (4.28) into (4.20) to obtain

$$I_3 = \sum_i \sum_j \left\{ \sum_k (\alpha_z w \delta_k \bar{\Pi}^k) + (\bar{\Sigma}_s^{ij} + F_s) \Pi_s \right.$$

+ Pressure Work Against Boundary Fluxes, (4.29)

so that the work done by the pressure forces on the horizontal flow is equal to the work done by the buoyancy forces, plus the rate of pressure work at the lateral boundaries - Conservation Property 4. The first two terms in (4.29) are the finite-difference representation of the first two terms on the right in (2.56).

We note in conclusion that in the case of no-flux or periodic conditions at the longitudinal boundaries and no-flux conditions at the latitudinal boundaries, the lateral boundary terms in (4.29) exactly vanish.

Section 5

SUMMARY AND CONCLUDING REMARKS

In this report we have presented a set of differential equations and boundary conditions suitable for forecasting the currents, temperature, salinity and density over both whole-oceans and limited ocean regions. We have also presented a spatial finite-difference representation of these equations. The finite-difference treatment of the temporal variation is presented in an accompanying report. In this final section we briefly summarize both the model differential equations and their finite-difference representation.

In Section 2 we described in detail the derivation of the model differential equations. We began by assuming that the Boussinesq approximation is appropriate, and we introduced a coordinate system based on the earth's geopotential surfaces and longitude and latitude defined in the usual manner in terms of these surfaces. Then, recognizing that the resolution of all important oceanic scales of motion by a finite-difference scheme is simply not possible, we introduced a parameterization of the effects of unresolved "sub-grid scale" transport on the resolved motions. The parameterization is based on a gradient diffusion hypothesis with an anisotropic diffusivity. The horizontal diffusivity is a function of a measure of the finite-difference grid spacing in the lateral plane, and the vertical diffusivity depends on the vertical variation of both the density and the horizontal velocity. Then we applied a thin-layer assumption, made the hydrostatic approximation and ignored

the variation of the coordinate system metric coefficients from their spherical thin-layer counterparts. Finally, we introduced a new vertical variable σ which varies from zero at the surface to one at the bottom, an appropriate equation of state, modifications to alleviate round-off errors, and the implementation of user specified poles.

We also described boundary conditions in Section 2. We specified that the forecast region will always be rectangular in λ and ϕ , and that land areas which might be located within the interior or at the boundaries of the forecast region will be depressed and covered with a thin layer of water. This treatment of land areas will greatly simplify the computer coding.

We concluded Section 2 with a brief discussion of some of the integral properties of the model differential equations which provide guidance in their finite-difference representation.

In Section 3 we presented a spatial finite-difference representation of the model equations. We described the staggered grid system and the motivation behind it. We obtained second-order accurate difference equations with the aid of a "box" approach. We also described the representation and implementation of the boundary conditions, including the introduction of mesh points just outside the forecast region boundaries.

Finally, in Section 4 we discussed the conservation properties of our finite-difference equations. In particular, we showed they conserve representations of heat and salt. We also showed that the advection terms

in the equations make no net contributions to appropriate representations of the volume integrals of the horizontal kinetic energy and the squares of temperature and salinity; this result frees our scheme from problems associated with "non-linear instability". To conclude Section 4, we showed that a representation of the rate of work done by the pressure gradients on the horizontal flow is equal to a natural representation of the rate of work done against the buoyancy forces, plus the rate of pressure work at the boundaries.

The second phase of the model development, which includes computer programming, debugging, and preliminary application of the model, is now underway. The program is being written carefully in a modular fashion to make modification simple, and we are emphasizing readability through the use of "top-down" programming techniques. During this phase, we are laying the computer code groundwork for what will be an effective, flexible, and efficient ocean forecasting tool.

Section 6

REFERENCES

1. Bryan, K., (1966), "A Scheme for Numerical Integration of the Equations of Motion on an Irregular Grid Free of Nonlinear Instability", Mon. Weather Rev., Vol. 94, No. 1.
2. Bryan, K. and Cox, M.D., (1972), "An Approximate Equation of State for Numerical Models of Ocean Circulation", J. Phys. Oceanogr., Vol. 2, No. 4.
3. Chen, C.T. and Millero, F.J., (1976), "The Specific Volume of Seawater at High Pressures", Deep-Sea Research, 23, 595-612.
4. Chen, C.T. and Millero, F.J., (1977), "Precise Equation of State of Seawater for Oceanic Ranges of Salinity, Temperature and Pressure", Deep-Sea Research, 24, 365-369.
5. Fofonoff, N.P., (1962), "Physical Properties of Sea Water", The Sea, Vol. 1, Interscience, N.Y.
6. Jerlov, N.G., (1961), "Optical Studies of Ocean Water", Rept. of Swedish Deep-Sea Exped., 3.
7. Kwak, D., Reynolds, W.C. and Ferziger, J.H., (1975), "Three-Dimensional Time Dependent Computation of Turbulent Flow", Report No. TF-5, Dept. of Mech. Eng., Stanford University.
8. Launder, B.E., (1974), "On the Effects of a Gravitational Field on the Turbulent Transport of Heat and Momentum", J. Fluid Mech., Vol. 67, Part 3.
9. Martin, P.J., (1976), "A Comparison of Three Diffusion Models of the Upper Mixed Layer of the Ocean", Naval Research Laboratory Memorandum Report 3399.

11. Mellor, G.L. and Yamada, T., (1974), "A Hierarchy of Turbulence Closure Models for Planetary Boundary Layers", J. Atmos. Sci., Vol. 32, p. 1791.
12. Piacsek, S.A. and Williams, G.P., (1970), "Conservation Properties of Convection Difference Schemes", J. Comp. Phy., Vol. 6, p. 392.
13. Roache, P.J., (1972), Computational Fluid Dynamics, Hermosa Publishers, Albuquerque, N.M.
14. Roberts, G.O. and Grabowski, W.J., (1978a), "A Sigma Coordinate Ocean Forecasting Computer Code, II. Time Representation and Stability Properties", in preparation.
15. Roberts, G.O. and Grabowski, W.J., (1978b), "Turbulence Parameterization for Ocean Forecasting Codes", in preparation.
16. Smagorinsky, J., Manabe, S. and Holloway, J.L., (1965), Mon. Weath. Rev., Vol. 93, p. 727.
17. Sverdrup, H.U., Johnson, M.W. and Fleming, R.H., (1942), The Oceans: Their Physics, Chemistry, and General Biology, Prentice-Hall, Englewood Cliffs, N.J.
18. Webster, C.A.G., (1964), "An Experimental Study of Turbulence in a Density Stratified Shear Flow", J. Fluid. Mech., Vol. 19, p. 2.
19. Woods, J.D., (1977), "Parameterization of Unresolved Motions", in Modelling and Prediction of the Upper Layer of the Ocean, Pergamon Press, E.B. Kraus, ed.